Resonant scattering of plasma sheet electrons leading to diffuse auroral precipitation: 1. Evaluation for electrostatic electron cyclotron harmonic waves

Binbin Ni,[1] Richard M. Thorne,[1] Richard B. Horne,[2] Nigel P. Meredith,[2] Yuri Y. Shprits,[1,3] Lunjin Chen,[1] and Wen Li[1]

Received 21 October 2010; revised 7 January 2011; accepted 8 February 2011; published 19 April 2011.

[1] Using statistical wave power spectral profiles obtained from CRRES and the latitudinal distributions of wave propagation modeled by the HOTRAY code, a quantitative analysis has been performed on the scattering of plasma sheet electrons into the diffuse auroral zone by multiband electrostatic electron cyclotron harmonic (ECH) emissions near $L = 6$ within the 0000–0600 MLT sector. The results show that ECH wave scattering of plasma sheet electrons varies from near the strong diffusion rate (timescale of an hour or less) during active times with peak wave amplitudes of an order of 1 mV/m to very weak scattering (on the timescale of >1 day) during quiet conditions with typical wave amplitudes of tenths of mV/m. However, for the low-energy (~100 eV to below 2 keV) electron population mainly associated with the diffuse auroral emission, ECH waves are only responsible for rapid pitch angle diffusion (occasionally near the limit of strong diffusion) for a small portion of the electron population with pitch angles $\alpha_{eq} < 20°$, dependent on electron energy and geomagnetic activity level. ECH scattering alone cannot account for the rapid loss of plasma sheet electrons during transport from the nightside to the dayside, nor can it explain the formation of the pancake electron distributions strongly peaked at $\alpha_{eq} > 70°$. Computations of the bounce-averaged coefficients of momentum diffusion and (pitch angle, momentum) mixed diffusion indicate that both mixed diffusion and energy diffusion of plasma sheet electrons due to ECH waves are very small compared to pitch angle diffusion and that ECH waves have little effect on local electron acceleration. Consequently, the multiple harmonic ECH emissions cannot play a dominant role in the occurrence of diffuse auroral precipitation near $L = 6$, and other wave-particle interaction mechanisms, such as whistler mode chorus-driven resonant scattering, are required to explain the global distribution of diffuse auroral precipitation and the formation of the pancake distribution in the inner magnetosphere.

Citation: Ni, B., R. M. Thorne, R. B. Horne, N. P. Meredith, Y. Y. Shprits, L. Chen, and W. Li (2011), Resonant scattering of plasma sheet electrons leading to diffuse auroral precipitation: 1. Evaluation for electrostatic electron cyclotron harmonic waves, *J. Geophys. Res.*, *116*, A04218, doi:10.1029/2010JA016232.

1. Introduction

[2] As an almost permanent feature in the Earth's ionosphere, the diffuse aurora reflects one of the most important loss processes of plasma sheet electrons, which supplies the majority of ionizing energy input into the high-latitude region during conditions of both low and high solar wind driving [e.g., *Sandford*, 1968; *Newell et al.*, 2009]. Diffuse auroral emissions, primarily resulting from the precipitation of 100s eV to a few keV electrons, can dramatically increase the conductivity of the ionosphere and thus provide an essential coupling between the magnetosphere and the middle atmosphere. Although both ions and electrons precipitate in the diffuse auroral zone, the average integral number flux of the precipitating auroral ions is typically 1 to 2 orders of magnitude less than that of the precipitating auroral electrons [*Hardy et al.*, 1985, 1989]. While it is generally accepted that the central plasma sheet provides the source of electrons for the diffuse aurora [*Lui et al.*, 1977; *Meng et al.*, 1979], there is no general consensus on the scattering mechanism(s) responsible for electron precipitation.

[3] Over many decades electrostatic electron cyclotron harmonic (ECH) waves have been proposed as a candidate for diffuse auroral electron precipitation through resonant cyclotron harmonic scattering (see the reviews by *Swift* [1981], *Kennel and Ashour-Abdalla* [1982], and *Coroniti*

[1]Department of Atmospheric and Oceanic Sciences, University of California, Los Angeles, California, USA.
[2]British Antarctic Survey, Cambridge, UK.
[3]Institute of Geophysics and Planetary Physics, University of California, Los Angeles, California, USA.

0148-0227/11/2010JA016232

[1985]). ECH emissions, also known as "n + 1/2" waves, occur within bands between the harmonics of the electron gyrofrequency, f_{ce}, with the dominant frequency often located around (n + 1/2) f_{ce} [e.g., *Kennel et al.*, 1970; *Fredricks and Scarf*, 1973; *Scarf et al.*, 1973; *Shaw and Gurnett*, 1975]. These waves propagate at very large angles with respect to the ambient magnetic field [e.g., *Gurnett and Bhattacharjee*, 2005]. ECH waves are generally thought to be driven by a loss cone instability of the source electron velocity distribution [e.g., *Young et al.*, 1973; *Ashour-Abdalla and Kennel*, 1978; *Horne*, 1989; *Horne et al.*, 1981, 2003]. While these electrostatic emissions have been detected at all local times and at all the latitudes up to ~45° [*Fredricks and Scarf*, 1973; *Shaw and Gurnett*, 1975], and are found over a wide range of geocentric distances of 4–12 R_E [*Kennel et al.*, 1970; *Roeder and Koons*, 1989], it has been established that the most intense emissions occur over the evening to dawn sector (2100–0600 MLT) at $4 < L < 8$ and are confined to within a few degrees of the magnetic equator [*Roeder and Koons*, 1989; *Paranicas et al.*, 1992; *Meredith et al.*, 2009].

[4] It was first suggested by *Kennel et al.* [1970] that ECH waves could provide a mechanism for pitch angle diffusion and turbulent energization of auroral zone electrons based on observations of large amplitudes (typically between 1 and 10 mV/m and occasionally up to 100 mV/m) for ECH emissions from the OGO-5 satellite. Using these amplitudes over the entire magnetic field line and focusing on one wave frequency at 1.5 f_{ce}, *Lyons* [1974] quantitatively evaluated the bounce-averaged diffusion coefficients for scattering in both energy and pitch angle. The results indicated that the ECH emissions reported by *Kennel et al.* [1970] could cause electron pitch angle scattering approaching the strong diffusion rate over the energy range from hundreds of eV to tens of keV, typical of those particles responsible for the diffuse aurora. However, the effectiveness of ECH scattering was challenged by *Belmont et al.* [1983], who pointed out that the stronger ECH events (>1 mV/m) occur less than 2% of the time compared to 88% occurrence of much weaker electric fields (<0.1 mV/m), based on a statistical analysis of the GEOS-2 data covering the 2200–0600 MLT sector and the magnetic latitudes within 3° of the magnetic equator. Since the ECH wave amplitude estimated by *Belmont et al.* [1983] for strong diffusion of ~1 keV electrons (≥2 mV/m) was not reached during most of the investigated time period (>91%), they concluded that some other mechanisms besides ECH waves should be included to account for the diffuse auroral electron precipitation. Predominance of more modest levels of ECH emissions similar to those reported by *Belmont et al.* [1983] was reported later by *Roeder and Koons* [1989] using the SCATHA and AMPTE data, by *Koons and Roeder* [1990] using the SCATHA data, and by *Paranicas et al.* [1992] using the CRRES data.

[5] However, a careful analysis of CRRES wave data by *Meredith et al.* [2000] led to a resurgence in interest of ECH scattering, when they established that ECH wave amplitudes following substorm activity were typically above 1 mV/m, whenever the spacecraft was close to the magnetic equator. Adopting a representative amplitude of 1 mV/m for active conditions, *Horne and Thorne* [2000] evaluated the bounce-averaged rates of pitch angle diffusion for representative ECH wave frequencies in each harmonic band. They found that the substorm-associated ECH waves have sufficient power to cause scattering near the loss cone at a rate comparable to strong diffusion limit for electrons below 500 eV. However, the magnitudes of diffusion coefficients and their variations with equatorial pitch angle are strongly dependent on adopted wave frequency and the wave normal angle distribution. For instance, their results suggested that waves with normalized wave frequencies $f/f_{ce} \leq 1.5$ could efficiently scatter plasma sheet electrons near the loss cone, but either waves with $f/f_{ce} > 1.8$ or a broad distribution of wave normal angles (≥0.5°) are required to pitch angle diffuse the electrons with higher equatorial pitch angles. This conclusion was confirmed by *Horne et al.* [2003] based on the analysis of wave propagation and resonant electron scattering for a weak substorm injection event.

[6] *Fontaine and Blanc* [1983] were among the first to model the convective transport and resonant diffusion of plasma sheet electrons to simulate the morphology and the dynamics of the diffuse auroral zone and compare their results with observations. By applying scattering at the strong diffusion limit as proposed by *Kennel* [1969], they found that the transport of plasma sheet electrons (~keV) and their pitch angle diffusion into the atmosphere loss cone could be the main causes for diffuse auroral precipitation. However, the strong diffusion assumption might overestimate the efficiency of wave-particle interactions. A similar conclusion was reached by *Chen and Schulz* [2001a, 2001b], who modeled the precipitating energy flux into the auroral ionosphere as a function of magnetic invariant latitude and MLT using a guiding center transport model of plasma sheet electrons under various rates of pitch angle diffusion. Scattering below the strong diffusion limit was needed to best simulate electron precipitations near dawn and in the morning quadrant.

[7] The above discussion indicates the importance of careful quantification of the scattering rates of plasma sheet electrons through wave-particle interactions with a more realistic wave model. The recent statistical study by *Meredith et al.* [2009] of the power spectral intensity of upper band chorus and ECH waves using the entire CRRES database provides a unique opportunity for quantifying the rates of plasma sheet electron loss due to ECH wave scattering. The CRRES database is therefore used here to evaluate resonant electron diffusion rates during quiet, moderate, and active conditions as a function of energy and pitch angle over each broad cyclotron harmonic band rather than at a particular frequency as done earlier by *Horne and Thorne* [2000]. Modeling the wave frequency distribution in each harmonic band between the electron gyrofrequency and below upper hybrid resonance frequency also allows us to determine the relative role of each ECH wave band for plasma sheet electron scattering.

[8] Another key parameter required for the evaluation of electron scattering rates is the wave normal angle distribution of ECH emissions. While it is generally agreed that ECH waves propagate highly obliquely with respect to the background magnetic field, precise angular distributions have not yet been obtained from observations. Instead, we will resort to theoretical modeling of the generation of ECH waves during cyclotron resonant instability with a modest electron loss cone distribution [*Fredricks*, 1971; *Young et al.*, 1973; *Ashour-Abdalla and Kennel*, 1978; *Horne*, 1989; *Horne et al.*, 1981, 2003]. Ray tracing simulation of wave

propagation and growth, similar to those of *Horne et al.* [2003], can therefore be employed to obtain the optimum equatorial wave normal angle and its variation during propagation to higher latitude for any ECH wave frequency of interest.

[9] Based on the above considerations, in the present study focusing on ECH wave-driven resonant scattering of plasma sheet electrons into the diffuse auroral zone, we first describe in section 2 a statistical model for the frequency spectrum of ECH wave power, using the same CRRES database as used by *Meredith et al.* [2009]. A wave normal angle model and its variation with latitude obtained using HOTRAY simulations are then developed in section 3. A brief summary of the quasi-linear formalism for reliable evaluation of resonant scattering by ECH waves is presented in section 4 along with the results of bounce-averaged quasi-linear diffusion coefficients for diffuse auroral electrons under different geomagnetic activity conditions. We discuss the results in section 5 and make the conclusions in section 6.

2. Frequency Spectrum of ECH Wave Power Based on the CRRES Observations

[10] As a nearly equatorially orbiting spacecraft, the Combined Release and Radiation Effects Satellite (CRRES) operated from 25 July 1990 through October 1991 in a highly elliptical geosynchronous transfer orbit with an initial apogee of 35,768 km, a perigee of 305 km, and an inclination of ~18°. With an orbital period of ~10 h, the CRRES satellite swept through the heart of the radiation belts every half orbit, and the Plasma Wave Experiment onboard provided a good wave database in the frequency range from 5.6 Hz to 400 kHz with high resolution in frequency and time and good sensitivity in amplitude for almost 15 months, covering the geocentric distances from $L = 1.05$ to $L = \sim 8$, and geomagnetic latitude range up to 30° [*Anderson et al.*, 1992; *Meredith et al.*, 2001, 2004, 2009].

[11] In the present study we use the same CRRES database for ECH waves as *Meredith et al.* [2009] and exclude the prenoon sector where the wave coverage was poor. In addition to binning the wave data as a function of half orbit (inbound and outbound) and L in a step of 0.1 L, *Meredith et al.* [2009] obtained the electric field intensities for the equatorial ECH waves (within 3° of the magnetic equator) in a step of 0.1 f_{ce} for the first harmonic band (f_{ce}–2 f_{ce}) and in a step of 0.2 f_{ce} for the three higher harmonic bands (2 f_{ce}–5 f_{ce}) to facilitate a detailed statistical spectral analysis during different geomagnetic activity levels. Since diffuse auroral precipitation is most intense over the midnight to dawn sector, coincident with the MLT locations of strongest ECH emissions, in this study we confine our attention to the statistical properties of ECH wave power spectral intensity in the 00–06 MLT interval. Basically, each individual wave profile is an average of the ECH wave intensities taken over 0.1 L. This corresponds to an integration time ranging from 4 to 8 min at $L = 4$ and $L = 6$, respectively. At any given L shell and for any given activity level the average profile is typically calculated from 30–100 individual wave profiles, although the number of individual profiles can be smaller at low L during geomagnetically quiet times. As a consequence, we have a reasonable number of wave events to perform a statistical analysis based on the CRRES wave measurements. We further average the wave spectral intensities over intervals of 0.5 L to obtain the representative wave power spectra at $4 \le L \le 6$ (for instance, averaging over $L = 3.8$–4.2 for the spectrum at $L = 4.0$, averaging over $L = 4.3$–4.7 for the spectrum at $L = 4.5$, etc).

[12] Figure 1 show the averaged ECH wave electric field spectral intensities (solid) as a function of frequency for each of the four harmonic bands, from top to bottom, under active ($AE^* > 300$ nT), moderate (100 nT < AE^* < 300 nT), and quiet ($AE^* < 100$ nT) conditions. Here AE^* is the maximum value of the AE index in the previous 3 h. A least squares Gaussian fit (dashed) is applied to the wave spectral intensity for each ECH wave band at $L = 4.0$, 4.5, 5.0, 5.5, and 6.0 (from left to right) for the above three geomagnetic activity levels. The most enhanced ECH emissions are seen during active conditions (top), the wave intensities decrease slightly for moderate conditions (middle) and are much weaker by at least an order of magnitude during quiet times (bottom). The first harmonic band generally contains the strongest emissions at each L shell, particularly for the geomagnetically active and moderate periods. The three higher harmonic bands exhibit weaker spectral intensities, with the second band frequently being the least intense. Wave intensities tend to maximize at L shell between 4.5 and 5.5 with a substantial decrease at low L, except for the most disturbed conditions ($AE^* > 300$ nT).

[13] To apply the least squares Gaussian fit, we have assumed that the ECH waves have a Gaussian frequency distribution given by

$$I_E(f) = A \exp\left[-\left(\frac{f - f_m}{\Delta f}\right)^2\right], (f_{lc} < f < f_{uc}) \qquad (1)$$

where I_E is the power spectral intensity of wave electric field (in $(\mathrm{mV/m})^2/\mathrm{Hz}$), f_m and Δf are the frequency of maximum wave power and bandwidth, respectively; f_{lc} and f_{uc} are the lower and upper cutoffs to the wave spectrum outside which the wave power is assumed to be zero, and A is a normalization factor given by

$$A = \frac{E_w^2}{\Delta f}\frac{1}{\pi^{3/2}}\left[\mathrm{erf}\left(\frac{f_m - f_{lc}}{\Delta f}\right) + \mathrm{erf}\left(\frac{f_{uc} - f_m}{\Delta f}\right)\right]^{-1}, \qquad (2)$$

where E_w is the wave electric field amplitude in units of mV/m and erf is the error function. Parameters for the Gaussian fits, including electric field amplitude (E_w), normalized peak frequency ($\overline{f_m} = f_m/f_{ce}$), and normalized bandwidth ($\overline{\Delta f} = \Delta f/f_{ce}$), are shown in Figure 2 as a function of L shell for all four harmonic bands under the three geomagnetic conditions. The profiles of wave amplitude shown on Figure 2 (top) confirm our findings above regarding the wave power dependence on geomagnetic activity, ECH wave band, and L shell. For example, the amplitudes of the first harmonic band always peak between 4.5 and 5.5 R_E, varying by more than 1 order of magnitude from just above 2.5 mV/m during active times to well below 0.2 mV/m during quiet times and being predominantly the largest among all the four bands for any geomagnetic condition. While the variations of the peak frequency and bandwidth for ECH waves are not as well organized with respect to spatial location and geomagnetic activity, which may be due to limited statistics, there are still a number of systematic

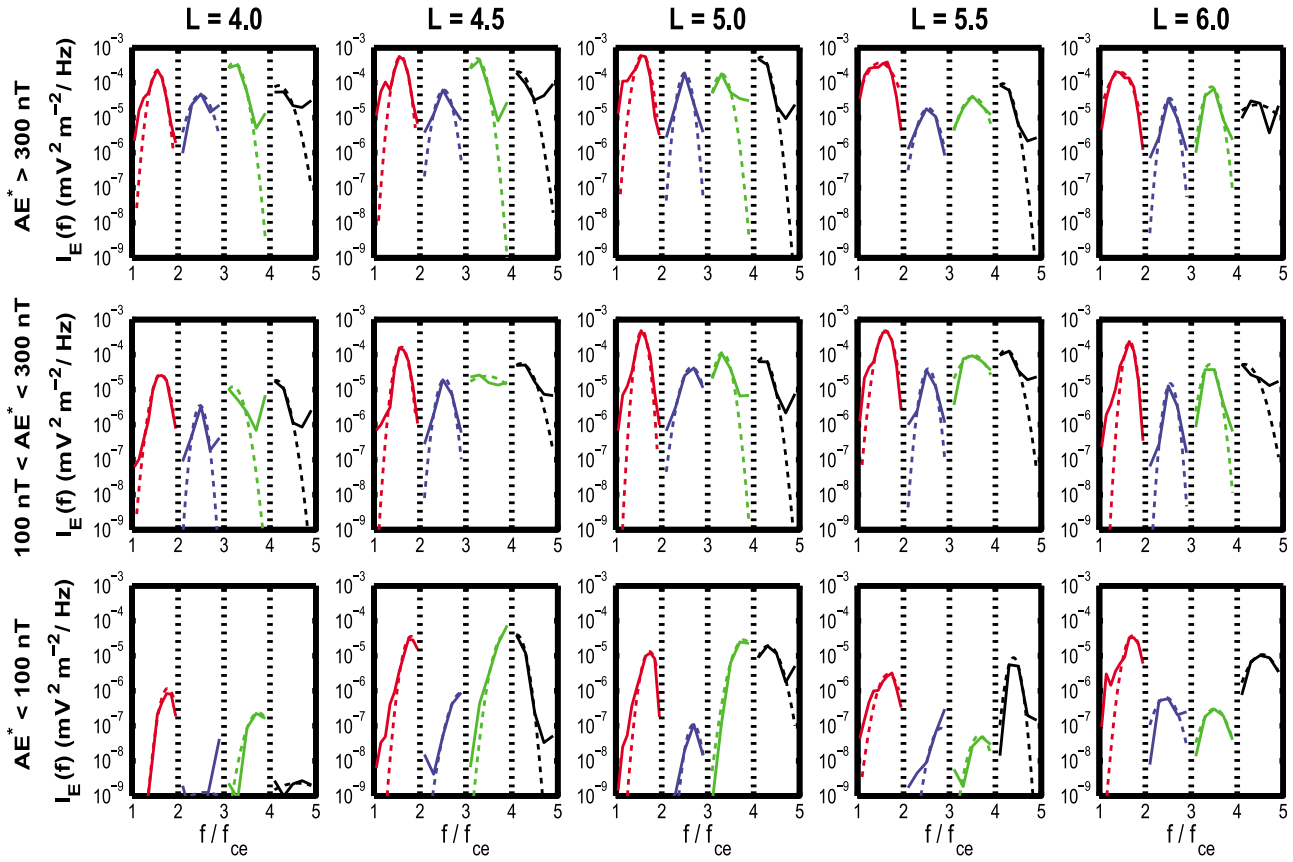

Figure 1. Averaged CRRES ECH wave electric field spectral intensities (solid) at L = 4.0, 4.5, 5.0, 5.5, and 6.0 as a function of normalized wave frequency for each of the four harmonic bands within 0000–0600 MLT sector under (top) active (AE^* > 300 nT), (middle) moderate (100 nT < AE^* < 300 nT), and (bottom) quiet (AE^* < 100 nT) conditions. Modeled Gaussian fits to the average spectra are shown as dashed curves.

features which are apparent: (1) as the geomagnetic activity becomes more intense, the peak frequencies for all the four bands tend to move to lower values in the band; (2) during active and moderate times the ECH wave emissions in the first two harmonic bands maximize near the center of the band, while in the higher harmonic bands the emissions maximize below the center of the band; and (3) the wave bandwidths for each of the four ECH harmonic bands are mostly confined between $\delta f = 0.1\ f_{ce}$ and $\delta f = 0.3\ f_{ce}$. All these characteristics, except those freshly described in the present study, are in a good agreement with the survey of ECH waves by *Meredith et al.* [2009].

[14] To quantify the rates of plasma sheet electron scattering by the observed electrostatic ECH waves, we concentrate on $L = \overline{6}$ and adopt the averaged Gaussian parameters ($E_w, \overline{f_m}, \overline{\Delta f}$) over the L shells of 4–6 to construct a representative frequency spectrum for each of the four ECH harmonic bands, which are tabulated in Table 1 for different levels of geomagnetic activity.

3. HOTRAY Simulation of the Latitudinal Distribution of ECH Waves

[15] A realistic determination of ECH wave-induced bounce-averaged diffusion coefficients also requires information on the wave propagation characteristics including wave normal angle and wave power spectrum along the particle bounce trajectory. This information, however, cannot be inferred readily from the CRRES observations, and there is very little detailed information in the literature. Consequently, to evaluate the propagation effects of ECH waves along the magnetic field, in this study we use the ray tracing HOTRAY code, which has been designed to trace any type of electrostatic or electromagnetic wave mode in a hot, magnetized, linearly unstable plasma containing several electron and ion species with Maxwellian type components at different temperatures [*Horn*e, 1989]. The HOTRAY code determines the raypath and any change in the wave normal angle by integrating Hamilton's equations for cold plasma so that wave frequency (ω) and wave number (k) remain real. The code also solves the hot plasma dispersion relation, including both Landau and up to 100 cyclotron harmonic resonances, at each step along the raypath for real ω to find the complex wave vector $\mathbf{k}$, the imaginary part ($\mathbf{k}_i$) of which is used to calculate the temporal wave growth/damping rate and path-integrated gain. For more details of the methodology for the HOTRAY code, readers are referred to a number of earlier studies [*Horne*, 1989; *Horne and Thorne*, 1993, 1994, 1997; *Horne et al.*, 2003].

[16] HOTRAY simulation in a heterogeneous magnetosphere requires specification of the spatial distribution of

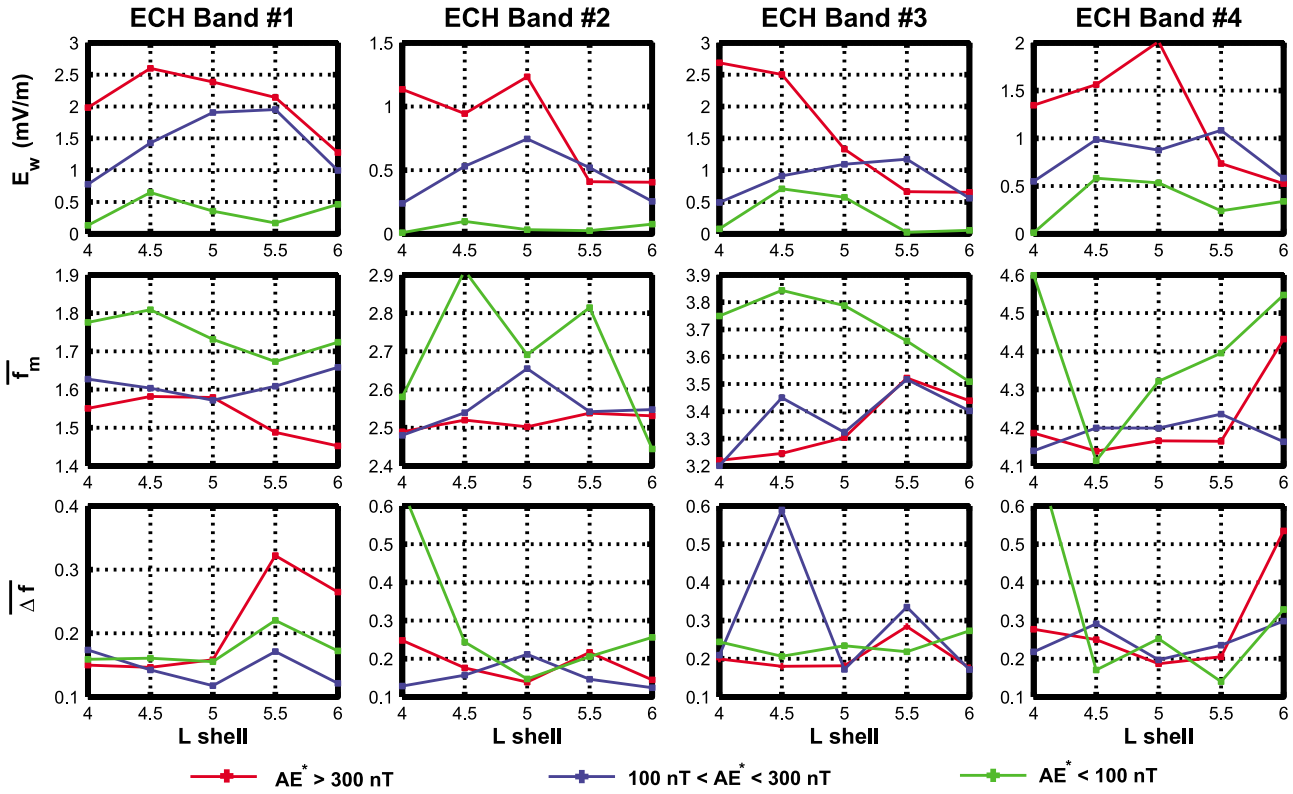

Figure 2. (top) Electric field amplitude, (middle) normalized peak frequency, and (bottom) normalized bandwidth obtained by applying the least squares Gaussian fit to the average spectra, as a function of L shell for the four ECH harmonic bands under three geomagnetic conditions.

background magnetic field and plasma density, together with phase space density of hot plasma sheet electrons responsible for wave excitation. In this study we use a dipole magnetic field model with the magnitude scaled by the observed equatorial magnetic field at the specified L shell. The total electron density and composition are determined from the components of the particle distribution function. The electron density is also assumed to be constant with zero gradient. Based on the averaged CRRES measurements near $L = 6$, Table 2 shows equatorial values of the ambient magnetic field and cold plasma density used to perform HOTRAY simulation of ECH waves under different levels of geomagnetic activity. The distribution of energetic electrons is modeled by a sum of subtracted Maxwellian components given by [e.g., *Ashour-Abdalla and Kennel*, 1978]

$$f_i(v_\perp, v_\parallel) = \frac{n_i}{\pi^{3/2}\alpha_{\perp i}^2\alpha_{\parallel i}}\exp\left(-\frac{v_\parallel^2}{\alpha_{\parallel i}^2}\right)\cdot\left[\Delta_i\exp\left(-\frac{v_\perp^2}{\alpha_{\perp i}^2}\right) + \frac{1-\Delta_i}{1-\beta_i}\left(\exp\left(-\frac{v_\perp^2}{\alpha_{\perp i}^2}\right)-\exp\left(-\frac{v_\perp^2}{\beta_i\alpha_{\perp i}^2}\right)\right)\right], \quad (3)$$

where the subscript i denotes the ith component of electrons, f_i is the phase space density (PSD), n_i is the electron density, $\alpha_{\perp i}$ and $\alpha_{\parallel i}$ are the thermal velocities perpendicular and parallel to the ambient magnetic field, and Δ_i and β_i determine the width and the depth of the loss cone, respectively.

Table 1. Electric Field Amplitude E_w, Peak Normalized Wave Frequency $\overline{f_m}$, and Normalized Bandwidth $\overline{\Delta f}$[a]

	Band 1	Band 2	Band 3	Band 4
	Active Conditions (AE > 300 nT)*			
E_w (mV/m)	2.0	0.8	1.5	1.0
$\overline{f_m}$	1.5	2.5	3.4	4.2
$\overline{\Delta f}$	0.2	0.2	0.2	0.25
	Moderate Conditions (100 nT < AE < 300 nT)*			
E_w (mV/m)	1.3	0.5	0.7	0.8
$\overline{f_m}$	1.6	2.55	3.4	4.2
$\overline{\Delta f}$	0.15	0.15	0.25	0.25
	Quiet Conditions (AE < 100 nT)*			
E_w (mV/m)	0.2	0.1	0.1	0.1
$\overline{f_m}$	1.75	2.7	3.65	4.35
$\overline{\Delta f}$	0.17	0.25	0.25	0.25

[a]Obtained by applying Gaussian fits to CRRES averaged wave intensity spectrum for each of the four ECH harmonic bands under different levels of geomagnetic activity

Table 2. Averaged Equatorial Values of Cold Plasma Density N_e, Ambient Magnetic Field B_0, the Ratio of Electron Plasma Frequency f_{pe} to Gyrofrequency f_{ce}, and the Gyroradius of the Cold Electrons ρ_e Based on the CRRES Measurements Around $L = 6$

	*AE** > 300 nT	100 nT < *AE** < 300 nT	*AE** < 100 nT
N_e (m^{-3})	2.88×10^6	5.52×10^6	1.69×10^7
f_{pe} (kHz)	15.24	21.1	36.89
B_0 (nT)	102.92	115.07	116.14
f_{ce} (kHz)	2.88	3.22	3.25
f_{pe}/f_{ce}	5.29	6.55	11.35
ρ_e (m)	32.7	29.3	29.0

[17] To model the hot electron distribution during geomagnetically disturbed condition, a typical ECH wave excitation event during orbit 486 on 10 February 1991 was investigated when CRRES was near the magnetic equator as shown in Figure 3a. The solid white line represents the equatorial electron gyrofrequency f_{ce}, the dotted lines above indicate the harmonics n f_{ce}, the dashed lines below are at 0.5 f_{ce}, 0.1 f_{ce}, and lower hybrid resonance frequency (f_{LHR}), and the solid red line shows the upper hybrid resonance frequency (f_{UHR}). Corresponding to the increase of *AE* from ~200 nT to >600 nT over the time period from ~1120 UT to ~1220 UT, outside the plasmasphere the wave power is considerably enhanced in several frequency bands. The waves between 0.1 and 1.0 f_{ce}, with a distinct gap at 0.5 f_{ce}, are typical of whistler mode chorus emissions, while the waves between n f_{ce} are ECH waves. The electron distribution measured at 1208 UT near L = 6, at a location very close to the magnetic equator during the enhancement of wave power, is shown in Figure 3b as a function of pitch angle for all the CRRES LEPA energy channels. The electron distributions at low energies (<1 keV) are nearly isotropic, however, the higher-energy electron distributions are anisotropic peaking at ~90° and show a certain loss cone feature around a few keV. Five components of the form (3) have been used to fit the observed electron pitch angle distribution over the velocity space shown in Figure 3c. Modeled contours (solid lines) of electron PSD are obtained by adjusting n_i, $\alpha_{\perp i}$, $\alpha_{\|i}$, Δ_i, and β_i to fit the observation (dotted lines), and the parameters are listed in Table 3 for HOTRAY simulations under both active and moderate conditions. For the thermal electron distribution model typical of quiet conditions, we adopt the loss cone (LC) distribution obtained by *Horne et al.* [2003] during a magnetically quiet CRRES orbit. The four thermal electron components used to model the electron distribution function with a partially filled loss cone are given in Table 4. For the coldest electron component ($T_\perp = T_\| = 1$ eV), the loss cone width and depth are set as 1.0 and 0.5, respectively, with its density inferred from the cold plasma density in Table 2 corresponding to different geomagnetic conditions.

[18] On the basis of the modeled electron distributions, HOTRAY code can solve the hot plasma dispersion relation for electrostatic ECH waves under different geomagnetic activities. As an example, the wave dispersion, temporal growth rates, group velocities, and estimated gain at L = 6 for all the four ECH harmonic bands are shown in Figure 4 for active times (*AE** > 300 nT). The HOTRAY dispersion relation solver was performed for four specific frequencies in each harmonic band by varying wave normal angle θ at the magnetic equator. The wave number k is normalized to the gyroradius of the coldest electrons ρ_e (also listed in Table 2) and remain almost constant with wave normal angle for any specified ECH wave frequency. The wave numbers generally tend to increase with higher harmonic bands, although the decrease in k for f/f_{ce} = 4.8 may be due to proximity to the upper hybrid resonance frequency f_{UHR}. In contrast, for each wave frequency the temporal growth rates (γ) change dramatically with wave normal angle, showing that ECH waves can only grow with highly oblique wave normal angles in a certain limited range. In general, the wave normal angles θ with maximum growth rate occur closer to 90° for higher ECH harmonic bands. In each harmonic band, the θ value corresponding to the peak growth rate is smallest near the central frequencies and migrates nearer to 90° with decreasing and increasing ECH normalized frequency. For a fixed wave normal angle, the growth rates peak at higher frequencies in each harmonic band, i.e., f/f_{ce} = 1.8, 2.8, 3.8, and 4.8. It is also important to note that the growth rates are substantially smaller at the lower frequencies in each harmonic hand with the peak values at least 1 order of magnitude lower than those for upper frequencies in the band.

[19] The group velocities (V_g) for ECH waves are relatively slow, varying from tens of km/s to hundreds of km/s and showing both frequency dependence and band dependence. With the exception of frequency close to f_{UHR}, the group velocities tend to decrease with higher harmonic bands. In each harmonic band, the group velocities for lower frequencies are smaller and show distinguishable variations with wave normal angle while for higher frequencies V_g exhibits little dependence on θ. Using the information of the wave growth rate and group velocity we can estimate the gain for each ECH wave frequency by assuming that they all stop at 3° of the magnetic equator at L = 6 and the magnitudes of γ and V_g do not change with latitude. Estimated gains show similar features as the temporal growth rate with respect to wave frequency and wave normal angle, indicating that ECH waves at lower frequencies in each harmonic band are very weak or cannot be excited in comparison with higher frequency components. Such characteristics in modeled wave intensity distribution, in addition to the statistics of ECH wave power spectrum shown in Figures 1 and 2, need to be considered when computing the diffusion coefficients which largely depend on the frequency spectrum of wave power.

[20] Since the peak growth rate occurs at different θ for different frequencies, it is expected that the most intense waves at each frequency tend to reach different maximum magnetic latitudes where the waves propagate exactly perpendicular to the ambient magnetic field. For instance, the growth rate peaks at θ = 89.3° for 1.5 f_{ce} but at 89.9° for 1.1 f_{ce} and 89.6° for 1.9 f_{ce}, suggesting that ECH waves at 1.5 f_{ce} propagate further in latitude along the field line than the other two frequencies before reflecting and propagating back toward the equator. Using the HOTRAY ray tracer for active conditions, Figure 5 shows the variation of magnetic latitude with group time during propagation for the four specific frequencies in each harmonic band. At each frequency the rays were launched from the magnetic equator with the wave normal angle corresponding to the maximum growth rate shown in Figure 4, but with various azimuth angles in the range of 0°–360° until the ray with the largest path-integrated gain was obtained for selection. The refraction by plasma density and magnetic field gradients results in changes in wave normal angle, which leads to reflection around the magnetic equator several times before the waves are strongly damped. Clearly, the maximum magnetic latitude for ECH wave propagation depends on both harmonic band and wave frequency. Strongly unstable ECH waves tend to be confined to within 2° of the magnetic equator in the first harmonic band, within 1.5° for the second and third bands, and within ~1° for the fourth band, in a good agreement with the observed wave characteristics [e.g., *Meredith et al.*, 2009]. Most of the waves with frequencies near the center of each band tend to propagate farthest away

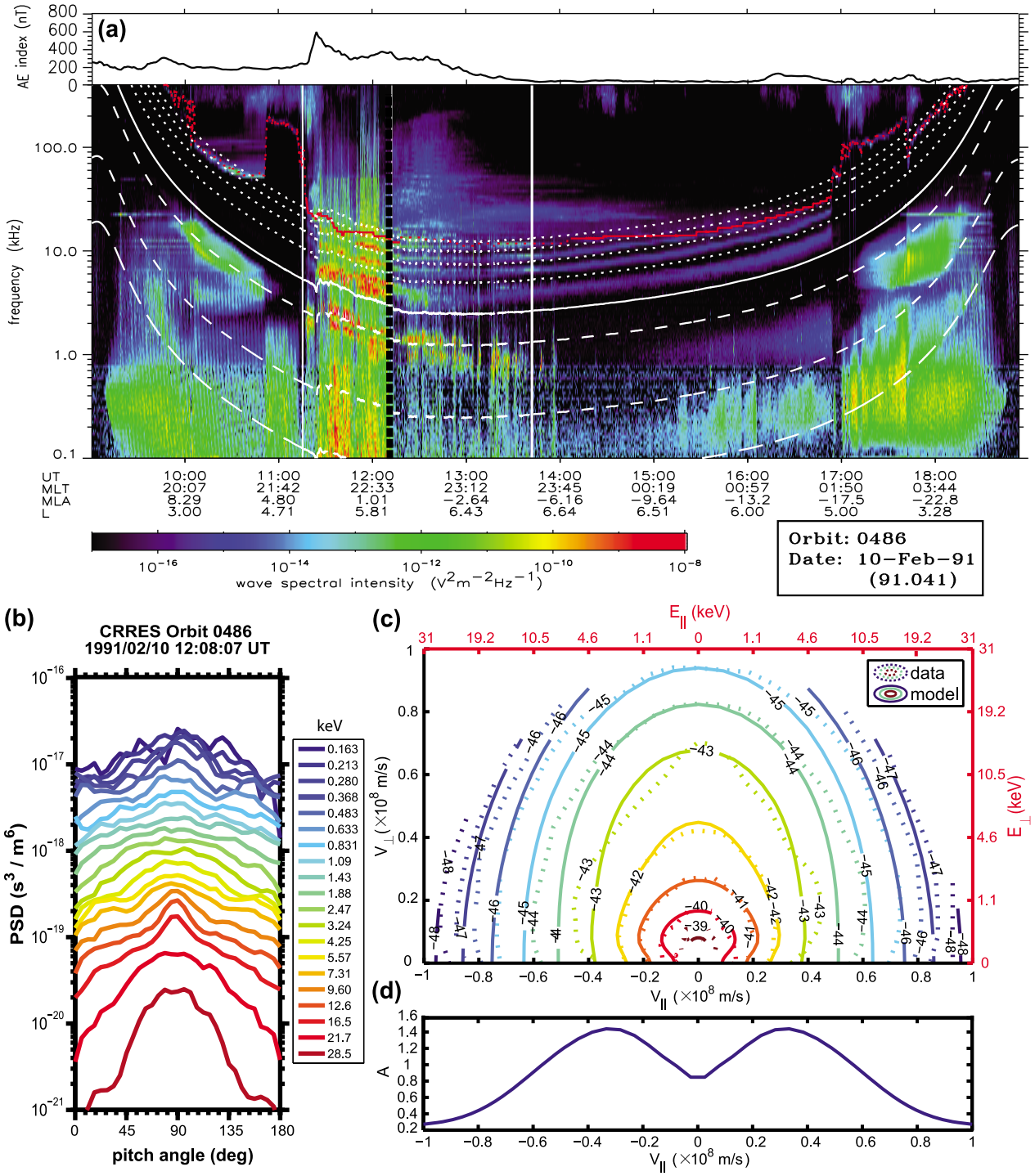

Figure 3. (a) (top) *AE* index as a function of Universal Time (UT); (bottom) wave spectral intensity (V^2 m^{-2} Hz^{-1}) from the electric field antenna on the CRRES plasma wave instrument as functions of wave frequency (kHz) and UT for orbit 486 on 10 February 1991. The red line indicates the upper hybrid resonance frequency f_{UHR}, and the white lines indicate equatorial electron gyrofrequency f_{ce} (solid), nf_{ce} (dotted), and 0.5 f_{ce}, 0.1 f_{ce} and lower hybrid resonance frequency f_{LHR} (dashed) from top to bottom. (b) The 5 min averaged electron phase space density (PSD) in s^3 m^{-6} as a function of equatorial pitch angle for various energy levels (0.163–28.5 keV) observed from the CRRES LEPA instrument starting at 1208 UT on 10 February 1991. (c) Contours of the electron PSD in ln(s^3 m^{-6}) as a function of perpendicular and parallel electron velocity (m/s) (or corresponding perpendicular and parallel kinetic energy (keV) indicated by the upper red axis). The dotted lines are from the electron PSD data from LEPA measurements and solid lines represent the contours of electrons PSD computed from the analytical model. (d) The electron anisotropy as a function of parallel electron velocity (m/s).

Table 3. Hot Electron Components Used to Model the Geomagnetically Active Time and Moderate Time Electron Distribution Function With a Loss Cone

Component	$T_\perp$ (eV)	$T_\parallel$ (eV)	N_e (m^{-3})	Δ	β
1	151	91	1.6×10^4	0.9	0.9
2	721	680	4.0×10^4	0.6	0.5
3	1821	1646	2.0×10^5	0.3	0.1
4	9319	5126	3.8×10^5	0.3	0.9
5	12609	10366	1.2×10^5	0.9	0.4

from the magnetic equator, consistent with a smaller initial wave normal angle at the equator (θ_e).

[21] While the HOTRAY results (Figure 5) agree favorably with the observed latitudinal distribution of ECH waves [e.g., *Roeder and Koons*, 1989; *Paranicas et al.*, 1992; *Meredith et al.*, 2009], variations of the raypath in radial distance can be significant, occasionally over 1 R_E. Nonetheless, based on the results shown in Figure 5, we make the following assumptions on the maximum latitude over which strong ECH waves are present: $\lambda_{max} = 3°$ if $\theta_e < 89.5°$; $\lambda_{max} = 2°$ if $89.5° \le \theta_e < 89.8°$; $\lambda_{max} = 1°$ if $\theta_e \ge 89.8°$. We further apply linear interpolation between the magnetic equator ($\theta_0 = \theta_e$) and λ_{max} ($\theta_0 = 90°$) to construct the latitudinal variation of wave normal angle during propagation for each considered wave frequency, as illustrated in Figure 6. While we have the least information for the angular width of ECH wave spectrum ($\delta\theta$), a corresponding linear fit is also assumed with peak value at the equator and $\delta\theta \to 0$ at λ_{max} (Figure 6, second row). Corresponding values of the parallel wave number ($k_{0,\parallel}$) and width in parallel wave number ($\delta k_\parallel$) are shown in Figure 6 (third row) and Figure 6 (fourth row), respectively. To obtain $k_{0,\parallel}$, we have used the HOTRAY hot plasma dispersion relation solver at the equator and taken the perpendicular wave number ($k_{0,\perp}$) unchanged with θ, which is generally the case based on the results shown in Figure 4. $\delta k_\parallel$ is determined by $\delta k_\parallel = k_{0,\perp}/\tan(\theta_0 - \delta\theta) - k_{0,\parallel}$ [*Horne and Thorne*, 2000]. The latitudinal variations of all these ECH wave parameters, modeled using the HOTRAY simulations, provide necessary inputs for an improved evaluation of bounce-averaged diffusion coefficients due to multiband ECH emissions.

[22] A similar simulation, using the HOTRAY dispersion relation solver and ray tracer, has also been made for moderate (100 nT < AE^* < 300 nT) and quiet (AE^* < 100 nT) conditions with the corresponding electron distribution (the results are not shown here). The main features for the propagation of the four ECH harmonic bands are very similar to those for active times, except that (1) the waves generally grow within a narrower latitude range around the magnetic equator, (2) the maximum wave growth rate drops considerably, and (3) the perpendicular and parallel wave numbers and the widths of wave number for wave power spectrum are different due to the differences in observed cold plasma density and ambient magnetic field at the equator.

4. Quantification of Bounce-Averaged Resonant Diffusion Coefficients

4.1. Methodology

[23] To quantify pitch angle scattering of plasma sheet electrons by highly oblique, broadband ECH emissions, with the observed wave power spectra and modeled wave normal angle distributions, we adopt the following procedure: (1) determine the bounce-averaged resonant diffusion rates at nine individual frequencies in each of the four harmonic bands using the corresponding averaged electric field amplitude, (2) apply the frequency distribution of wave power to obtain approximately weighted diffusion coefficients for each ECH harmonic band, and (3) sum the contribution from each band to obtain the net diffusion rates of diffuse auroral electrons by multiband ECH emissions.

[24] Based on the work by *Lyons* [1974], the local pitch angle diffusion coefficient for electrons due to electrostatic ECH waves (in units of s^{-1}) is given by

$$D_{\alpha\alpha} = \sum_{N=-\infty}^{+\infty} \int k_\perp dk_\perp \left[\Psi_{N,k} \left(\frac{N\Omega_e/\omega_k - \sin^2\alpha}{\sin\alpha\cos\alpha} \right)^2 \right]_{k_\parallel = k_{\parallel,res}} \quad (4)$$

with

$$\Psi_{N,k} = \frac{1}{4\pi} \frac{e^2}{m_e^2} \frac{|E_k|^2}{V} \left(\frac{\omega_k}{|k|} \right)^2 \frac{J_N^2(k_\perp v_\perp/\Omega_e)}{v^4 |v_\parallel - \partial\omega_k/\partial k_\parallel|}, \quad (5)$$

where $k_\perp$ and $k_\parallel$ are the components of the wave vector perpendicular and parallel to the ambient magnetic field $\mathbf{B}_0$, respectively, $k_{\parallel,res} = (\omega_k - N\Omega_e/\gamma)/v_\parallel$ is the resonant parallel wave number, $\Omega_e = |eB_0/m_e|$ is the angular electron gyrofrequency, ω_k is the wave frequency as a function of $\mathbf{k}$, $\gamma = (1 - v^2/c^2)^{-1/2}$ is the Lorentz factor with v as the electron velocity and c the speed of light, α is the electron pitch angle, V is the plasma volume, e/m_e is the electron charge to mass ratio, and J_N is the Bessel function of order N. Assuming that the parallel group velocity is small compared to the electron parallel velocity (i.e., $\partial\omega_k/\partial k_\parallel \ll v_\parallel$) and that the electric field spectrum has the form of

$$|E_k|^2 = Ck_\perp^2 \exp\left[-\left(\frac{k_\perp}{k_{0,\perp}} \right)^2 \right] \cdot \left\{ \exp\left[-\left(\frac{k_\parallel - k_{0,\parallel}}{\delta k_\parallel} \right)^2 \right] + \exp\left[-\left(\frac{k_\parallel + k_{0,\parallel}}{\delta k_\parallel} \right)^2 \right] \right\} \quad (6)$$

with a normalization constant

$$C = \frac{4\pi^{3/2}}{k_{0,\perp}^4 \delta k_\parallel} V |E_w|^2 \quad (7)$$

obtained from

$$\int |E_w|^2 dr = \frac{1}{8\pi^3} \int |E_k|^2 dk,$$

Table 4. Hot Electron Components Used to Model the Geomagnetically Quiet Time Electron Distribution Function With a Loss Cone

Component	$T_\perp$ (eV)	$T_\parallel$ (eV)	N_e (m^{-3})	Δ	β
1	150	30	1.2×10^5	1.0	0.5
2	300	300	10^5	0.3	0.2
3	1800	50	8.0×10^3	1.0	0.5
4	6200	4000	4.0×10^4	0.6	0.2

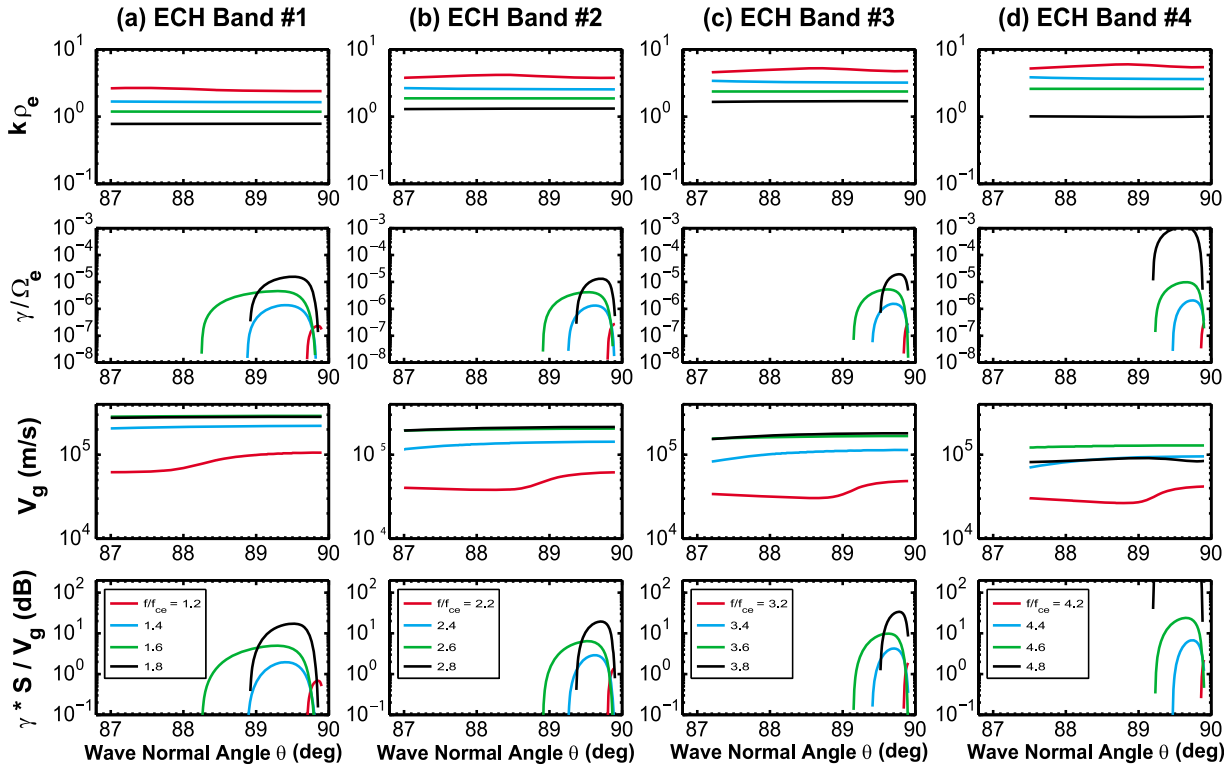

Figure 4. An example plot showing the wave number (k), temporal growth rate (γ), group velocity (V_g), and estimated gain as a function of wave normal angle at $L = 6$ for all four ECH harmonic bands under active conditions ($AE^* > 300$ nT). Calculations using HOTRAY hot plasma dispersion relation solver are performed for four specific wave frequencies in each ECH harmonic band.

Horne and Thorne [2000] developed equation (4) into a modified version:

$$D_{\alpha\alpha} = \frac{\sqrt{\pi}}{2}\frac{e^2}{m_e^2}\frac{|E_w|^2}{k_{0,\perp}^2\delta k_{\parallel}}\frac{\exp(-\mu)}{v^5\cos\alpha} \cdot \sum_{N=-\infty}^{+\infty}\left(\frac{N\Omega_e/\gamma - \omega_k\sin^2\alpha}{\sin\alpha\cos\alpha}\right)^2 \cdot I_N(\mu)\left\{\exp\left[-\left(\zeta_N^-\right)^2\right] + \exp\left[-\left(\zeta_N^+\right)^2\right]\right\}, \quad (8)$$

where $k_{0,\perp}$ and $k_{0,\parallel}$ are the wave number perpendicular and parallel to the ambient magnetic field $\mathbf{B}_0$, respectively, corresponding to the peak of the wave power, $\delta k_{\parallel}$ is the width of the wave spectrum distribution over parallel wave number, N is the resonance order associated with the resonance condition and the summation includes all the possible resonance harmonics, $I_N(\mu)$ is the modified Bessel function with the argument $\mu = k_{0,\perp}^2 v_{\perp}^2/(2\Omega_e^2)$, and

$$\zeta_N^{\pm} = \frac{\omega_k - N\Omega_e/\gamma}{\delta k_{\parallel} v\cos\alpha} \pm \frac{k_{0,\parallel}}{\delta k_{\parallel}}.$$

To obtain the values of the argument μ of the Bessel function, the perpendicular wave number $k_{0,\perp}$ is computed from the HOTRAY hot plasma dispersion relation solver for electrostatic waves and the perpendicular electron velocity $v_{\perp}$ is evaluated from the given kinetic energy and pitch angle of electrons. Based on equation (8) for $D_{\alpha\alpha}$, local pitch angle–momentum mixed diffusion rate $D_{\alpha p}$ and momentum diffusion rate D_{pp} can be obtained by [e.g., *Lyons*, 1974; *Glauert and Horne*, 2005; *Albert*, 2007]

$$D_{\alpha p} = D_{\alpha\alpha}\left[\frac{\sin\alpha\cos\alpha}{N\Omega_e/(\gamma\omega_k) - \sin^2\alpha}\right],$$
$$D_{pp} = D_{\alpha\alpha}\left[\frac{\sin\alpha\cos\alpha}{N\Omega_e/(\gamma\omega_k) - \sin^2\alpha}\right]^2. \quad (9)$$

Bounce-averaging the local diffusion rates over the electron bounce trajectory in a dipole magnetic field yields [e.g., *Lyons et al.*, 1972; *Glauert and Horne*, 2005; *Shprits et al.*, 2006; *Summers et al.*, 2007]

$$\langle D_{\alpha\alpha}\rangle = \frac{1}{S(\alpha_{eq})}\int_0^{\lambda_m} D_{\alpha\alpha}(\alpha)\frac{\cos\alpha\cos^7\lambda}{\cos^2\alpha_{eq}}d\lambda, \quad (10)$$

$$\langle D_{\alpha p}\rangle = \frac{1}{S(\alpha_{eq})}\int_0^{\lambda_m} D_{\alpha p}(\alpha)\frac{\sin\alpha\cos^7\lambda}{\sin\alpha_{eq}\cos\alpha_{eq}}d\lambda, \quad (11)$$

$$\langle D_{pp}\rangle = \frac{1}{S(\alpha_{eq})}\int_0^{\lambda_m} D_{pp}(\alpha)\frac{\sin^2\alpha\cos^7\lambda}{\sin^2\alpha_{eq}\cos\alpha}d\lambda, \quad (12)$$

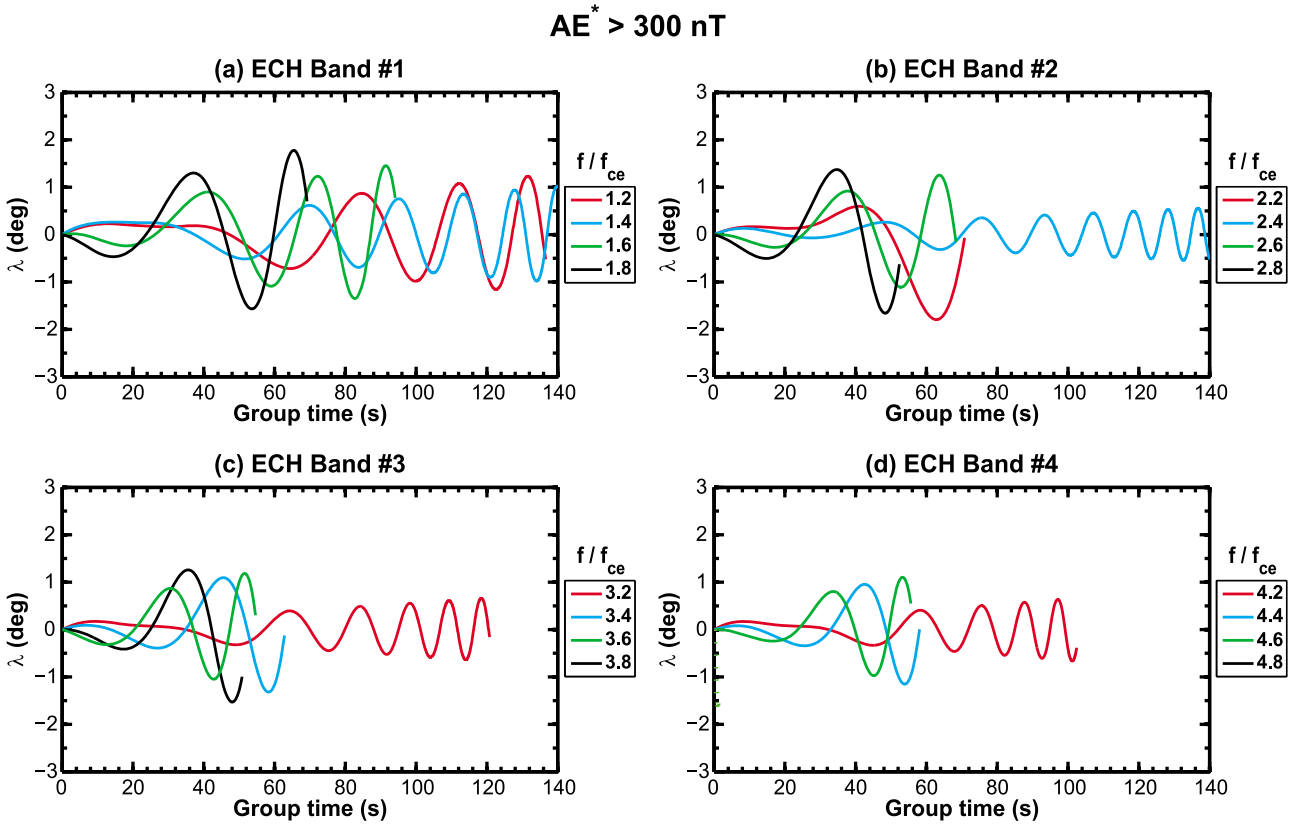

Figure 5. HOTRAY calculations of the variations of latitude along the raypath as a function of wave group time at $L = 6$ for ECH waves in four harmonic bands under active conditions ($AE^* > 300$ nT). In each harmonic band, four frequencies are specified for ray tracing.

where $S(\alpha_{eq}) = 1.3 - 0.56 \sin \alpha_{eq}$ [*Hamlin et al.*, 1961], α_{eq} is the equatorial pitch angle associated with local pitch angle α by

$$\sin^2 \alpha = \frac{\sqrt{1 + 3\sin^2 \lambda}}{\cos^6 \lambda} \sin^2 \alpha_{eq},$$

λ is the magnetic latitude, and λ_m is the upper limit of magnetic latitude determined either by the mirror latitude of the electrons or the maximum latitude of the wave occurrence. A constant cold electron density model with latitude is also adopted, which is reasonable for ECH waves mainly confined within 3° of the equator [e.g., *Meredith et al.* 2009].

[25] Equations (8)–(12) can readily be applied to evaluate the bounce-averaged resonant diffusion coefficients for any specified frequency once the wave electric field spectrum and wave normal angle distribution are available [*Horne and Thorne*, 2000]. Theoretically, quantification of diffusion rates requires integration over the entire ECH frequency band, which is dependent on solving the complicated hot plasma dispersion relation with expensive CPU time. Alternatively, we use the observed statistical wave power spectrum to introduce reasonable weighting factors for the diffusion rates at each wave frequency to provide a feasible approximate method to calculate the overall diffusion coefficients efficiently. Specifically, in the present study, for each harmonic band the overall bounce-averaged diffusion coefficients are computed by

$$\langle D \rangle_{overall} = \sum_{j=1}^{M} R_j \langle D \rangle_j \tag{13}$$

with the weighting factor for the jth wave frequency given by

$$R_j = \frac{(I_E)_j}{\sum_{j=1}^{M} (I_E)_j}. \tag{14}$$

Here M is the number of frequency considered in each band ($M = 9$ in this study by choosing frequencies normalized to f_{ce} from 1.1 to 1.9 with a step of 0.1 for the first harmonic band, from 2.1 to 2.9 with a step of 0.1 for the second harmonic band, and so on), $\langle D \rangle_j$ is the bounce-averaged diffusion rate due to the jth wave frequency, and $(I_E)_j$ is the electric field intensity for the jth wave frequency determined from the Gaussian functions described in Table 1 with respect to different geomagnetic activity levels. In order to take into account the effects of wave propagation along the field line, we adopt the maximum magnetic latitude modeled by the HOTRAY code as the upper limit for the integration in equations (10)–(12) and include the latitudinal dependence of wave power variation with wave normal angle.

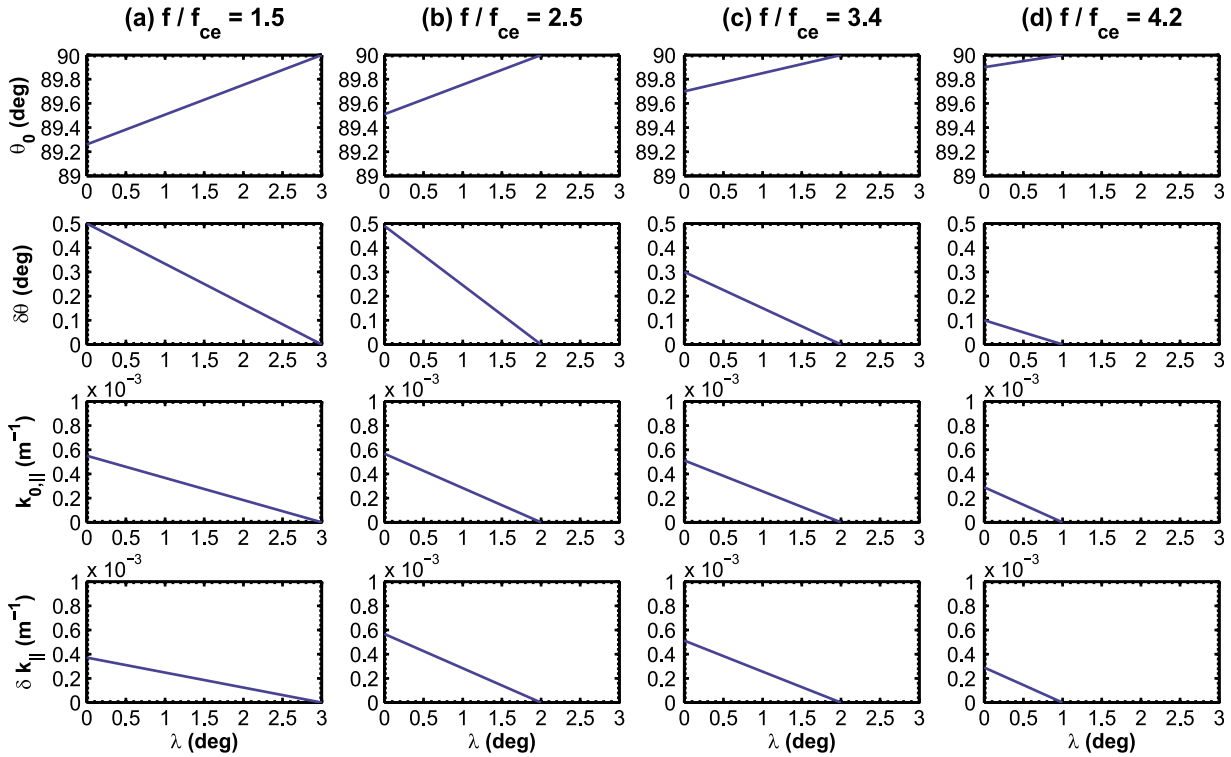

Figure 6. Examples of the modeled latitudinal distribution of wave normal angle distribution including peak wave normal angle (θ_0) and normal angle width ($\delta\theta$) and corresponding variations in peak value ($k_{0,\|}$) and width ($\delta k_{\|}$) of the parallel wave number at $L = 6$ for four specific wave frequencies, f/f_{ce} = 1.5, 2.5, 3.4, and 4.2.

This is a major improvement compared to the earlier calculations of *Horne and Thorne* [2000], who assumed that the local diffusion coefficient was approximately constant over a certain narrow equatorial latitude range and neglected any variations due to latitudinal changes in pitch angle and wave normal angle. Since the highest frequency waves considered lie between $4 < f/f_{ce} < 5$, contributions from $N = -10$ to $N = 10$ cyclotron harmonic resonances and Landau resonance $N = 0$ are included to encompass the dominant contributions to the scattering.

4.2. Model Results

[26] Figure 7 shows the bounce-averaged pitch angle diffusion rates at $L = 6$, as a function of equatorial pitch angle α_{eq} and kinetic energy E, at the nine frequencies in the first harmonic band under active conditions ($AE^* > 300$ nT). Initially, the electric field amplitude is taken as 1 mV/m for each frequency. The calculations are performed for 89 values of α_{eq} from 1° to 89° and 41 electron energies with logarithmically even spacing between 10 eV and 100 keV. Pitch angle diffusion coefficients for energies above ~10 keV due to ECH waves are well below 10^{-6} s^{-1} (a timescale of ~10 days or more), suggesting that ECH waves play a negligible role in scattering loss of these higher-energy plasma sheet electrons in the magnetosphere. For electrons below 10 keV, the magnitudes of the diffusion rates are strongly dependent on kinetic energy, ECH wave frequency, and equatorial pitch angle. For electrons with energies <100 eV, pitch angle scattering by ECH waves is negligible because the parallel wave numbers $k_{\|,res}$ required to resonate with these very low energy electrons are generally outside the limited parallel wave number spectrum for these frequencies. ECH wave-induced pitch angle diffusion near the loss cone become important when E > 100 eV. The strongest scattering occurs between ~100 eV and ~2 keV, depending on the normalized wave frequency. The peak values of $\langle D_{\alpha\alpha}\rangle$ near the loss cone are well above 10^{-5} s^{-1} up to several times 10^{-4} s^{-1}, indicating that ECH emissions can cause efficient precipitation loss of these relatively low energy plasma sheet electrons on a timescale of hours. Intense pitch angle scattering by ECH waves tends to be well confined to equatorial pitch angles below ~30°, but also shows strong frequency dependence. Specifically, for f/f_{ce} = 1.1–1.4 intense pitch angle diffusion ($\langle D_{\alpha\alpha}\rangle > 10^{-5}$ s^{-1}) only occurs within $\alpha_{eq} = 10^0$, while efficient scattering can extend to $\alpha_{eq} = 20°$ for f/f_{ce} = 1.5–1.7 and well above $\alpha_{eq} = 20°$ for f/f_{ce} = 1.8–1.9. The tendency for higher frequency ECH waves to resonate with higher energy plasma sheet electrons is mainly due to the decrease in parallel wave numbers with increased wave frequency (Figure 4). In the first harmonic band, the resonance harmonics $N = 1$ and 2 control the main features of bounce-averaged pitch angle diffusion coefficients. Contributions from the other cyclotron resonance harmonics and Landau resonance ($N = 0$) are considerably smaller.

[27] Taking into account the statistical properties (Table 1 and Figure 1) of the ECH wave power spectrum and applying the weighting method described by equations (13) and (14) to the diffusion rate matrices corresponding to the nine individual ECH wave frequencies (Figure 7), we obtain the weighted $\langle D_{\alpha\alpha}\rangle$ for the first ECH harmonic band shown

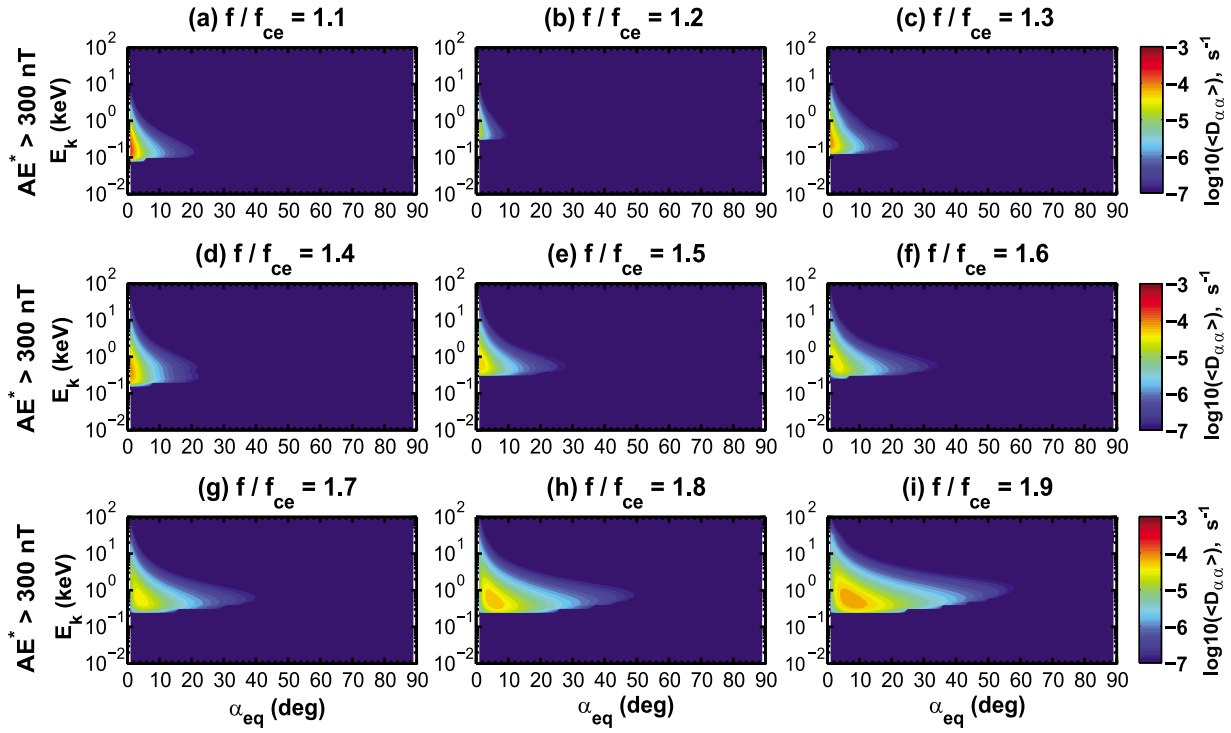

Figure 7. Bounce-averaged pitch angle diffusion coefficients as a function of equatorial pitch angle and electron kinetic energy for ECH waves at the indicated nine individual frequencies in the first harmonic band under active conditions ($AE^* > 300$ nT). A nominal electric field amplitude of 1 mV/m is taken for each frequency at $L = 6$.

in Figure 8a. Similar results are also shown for the other three harmonic bands for three levels of geomagnetic activity in Figures 8b, 8c, and 8d. It is clear that different harmonic bands make different contributions to scattering loss of plasma sheet electrons, each strongly dependent on the level of geomagnetic activity. During active conditions, the first band can induce efficient precipitation of electrons with energies between ~100 eV and ~5 keV for $\alpha_{eq} < 30°$. Pitch angle diffusions by the other three bands are less pronounced than the first harmonic band and are also generally confined to 100 eV < E ≤ ~2 keV with $\alpha_{eq} < 20°$. For intermediately disturbed periods (100 nT < AE^* < 300 nT), the diffusion coefficients show noticeable drops in magnitude for plasma sheet electrons of 100s eV to a few keV, compared to those for active times, mainly due to the lower intensity of ECH emissions (~1 mV/m) during moderate conditions. When the geomagnetic activity is quiet (AE^* < 100 nT), the weighted values of $\langle D_{\alpha\alpha}\rangle$ decrease by at least 1 order of magnitude for all the four ECH harmonic bands, mainly due to the sharp reductions in wave intensity. The maximum decrease (by a factor of at least 100) occurs for the first ECH harmonic band, consistent with the largest drop in averaged wave amplitude from 2 mV/m during active times to 0.2 mV/m during quiet times. Under geomagnetically quiet conditions, the ECH waves tend to undergo resonant interactions with the lower-energy electrons compared to moderate and active conditions, mainly attributed to changes in the background plasma (both cold and hot) distribution and ambient magnetic field.

[28] The total (net) bounce-averaged pitch angle diffusion coefficients due to all four ECH harmonic bands are shown in Figure 9 as a function of equatorial pitch angle and kinetic energy under different geomagnetic activity conditions, together with the bounce-averaged coefficients for momentum diffusion and pitch angle–momentum mixed diffusion. Figure 9 demonstrates that pitch angle scattering of plasma sheet electrons by the multiple banded ECH emissions is strongest with a typical scattering timescale of 1 h during active times ($AE^* > 300$ nT), moderately strong with a timescale of several hours for less disturbed conditions (100 nT < AE^* < 300 nT), and weakest (timescale above 1 day or more) during quiet periods ($AE^* < 100$ nT). Most intense scattering losses by ECH waves occur for plasma sheet electrons in the energy range of ~100 eV to ~5 keV during geomagnetically disturbed activities (AE^* > 100 nT). It is also clear that momentum diffusion rates and mixed rates are very small for all the levels of geomagnetic activity. Generally, $\langle D_{\alpha\alpha}\rangle > |\langle D_{\alpha p}\rangle| > \langle D_{pp}\rangle$, which can also be inferred from equation (9). The signs for $\langle D_{\alpha p}\rangle$ are shown in Figure 9 (fourth row) corresponding to the three different geomagnetic conditions.

[29] More detailed examination of pitch angle scattering plasma sheet electrons by ECH waves is shown in Figure 10 for five specific energies covering the range from 200 eV to 5 keV. For each energy we plot both the net values of $\langle D_{\alpha\alpha}\rangle$ due to the entire ECH emissions and the $\langle D_{\alpha\alpha}\rangle$ for each individual band to explore the relative roles of ECH wave harmonic bands. To investigate the efficiency of ECH waves in driving the precipitation loss of plasma sheet

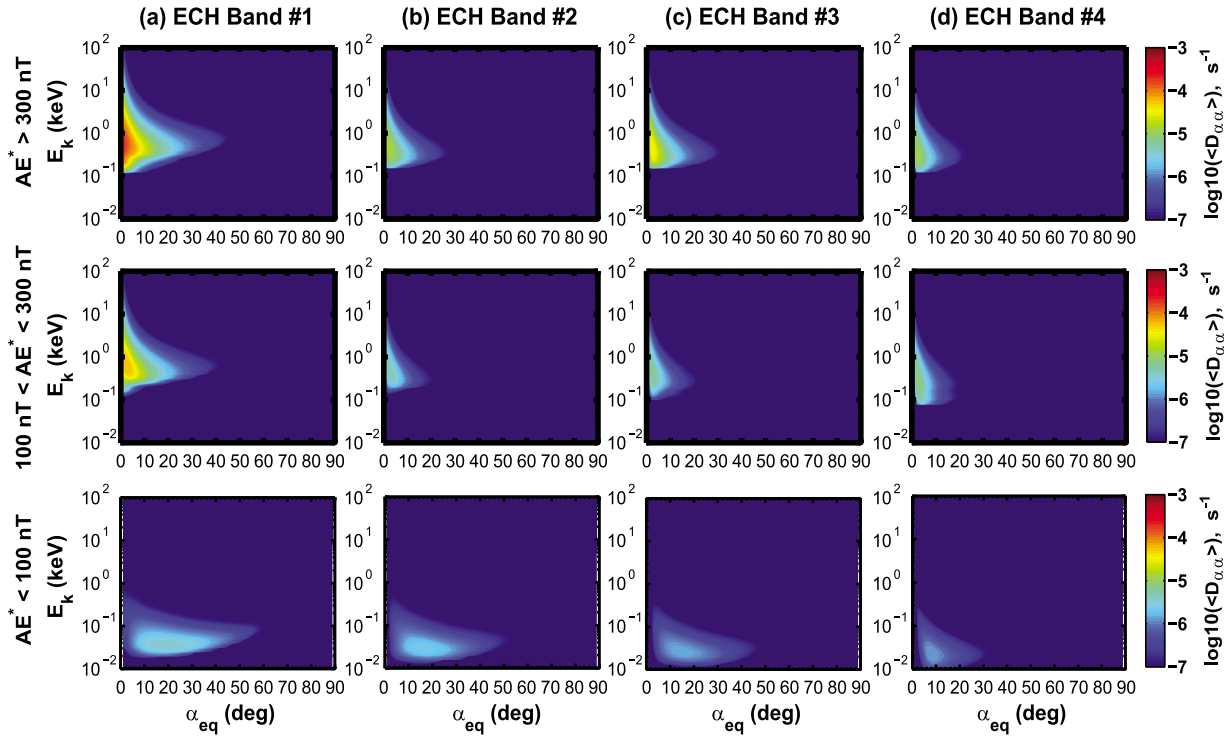

Figure 8. Weighted bounce-averaged pitch angle diffusion coefficients as a function of both equatorial pitch angle and electron kinetic energy for each of the four ECH harmonic bands at $L = 6$ corresponding to all the three geomagnetic activity conditions.

electrons, we also compare the coefficients with the strong diffusion rate (shown as horizontal dotted lines) determined by [*Summers and Thorne*, 2003]

$$D_{SD} \approx \frac{9.44}{L^4}\left(\frac{4L}{4L-3}\right)^{1/2}\frac{\left[\overline{E}\left(\overline{E}+2\right)\right]^{1/2}}{\overline{E}+1}, \qquad (15)$$

where L is the magnetic shell and $\overline{E} = E/(m_e c^2)$ is the electron kinetic energy in units of its rest energy. During active times, for electrons of energies between 200 eV and 1 keV (Figures 10a–10c) ECH wave-induced pitch angle diffusion approaches the regime of strong diffusion near the loss cone, which suggests that these low-energy electrons can be rapidly scattered into the atmosphere (within 1 or 2 h) and thus contribute to the diffuse aurora. The rates of scattering near the loss cone peak between 500 eV and 1 keV and then decrease as electron energy increases (Figure 10d), becoming inefficient for electrons >5 keV (Figure 10e). Efficient ECH wave scattering is also limited to $\alpha_{eq} < 20°$. Under moderately disturbed conditions, the rate of electron scattering by ECH waves drops well below the strong diffusion level, and the corresponding resonant plasma sheet electrons should exhibit only partially filled loss cones, whereas scattering under quiet conditions is much weaker and consistent with weak diffusion. These features are consistent with those obtained earlier using representative single-frequency ECH wave information [*Horne and Thorne*, 2000, Figure 1] in that ECH wave induced plasma sheet electron scattering is generally below the strong diffusion limit and in that there is little scattering for electrons with $\alpha_{eq} > 30°$, suggesting that ECH wave scattering alone cannot account for the formation of pancake distribution which typically exhibits a depleted electron population for $\alpha_{eq} < 70°$. More specifically, while the scattering rates near the loss cone in Figure 1 of *Horne and Thorne* [2000] are qualitatively similar to our results for moderately disturbed conditions, i.e., ~10^{-5} s^{-1} for 200 eV, ~10^{-4} s^{-1} for 500 eV, and between 10^{-5} and 10^{-4} s^{-1} for 1 and 2 keV, our results are somewhat smaller probably due to the inclusion of changes in wave normal angle with latitude, since ECH waves are unable to resonate with diffuse auroral electrons as the wave normal angle goes to 90°. In general, the largest diffusion coefficients originate from emissions in the first ECH harmonic band. Higher harmonic bands also contribute to resonant scattering of plasma sheet electrons, the magnitude of which largely depends on their averaged wave amplitudes relative to the first harmonic band.

5. Discussion

[30] A recent survey of upper band chorus and ECH waves using the CRRES database [*Meredith et al.*, 2009] described the global morphology of the waves, together with their dependence on geomagnetic activity, and noted the similarity to the global morphology of diffuse aurora. Intensities of both ECH waves and diffuse aurora peak during active conditions in the evening to dawn sector at $4 < L < 7$ and exhibit a minimum in the dusk quadrant [*Petrinec et al.*, 1999; *Anderson et al.*, 2001; *Meredith et al.*, 2009; *Newell et al.*, 2009]. It was also suggested by *Meredith et al.* [2009] that under active conditions both upper band chorus and ECH waves might be responsible for strong diffusion scattering of plasma sheet electrons and thus both waves

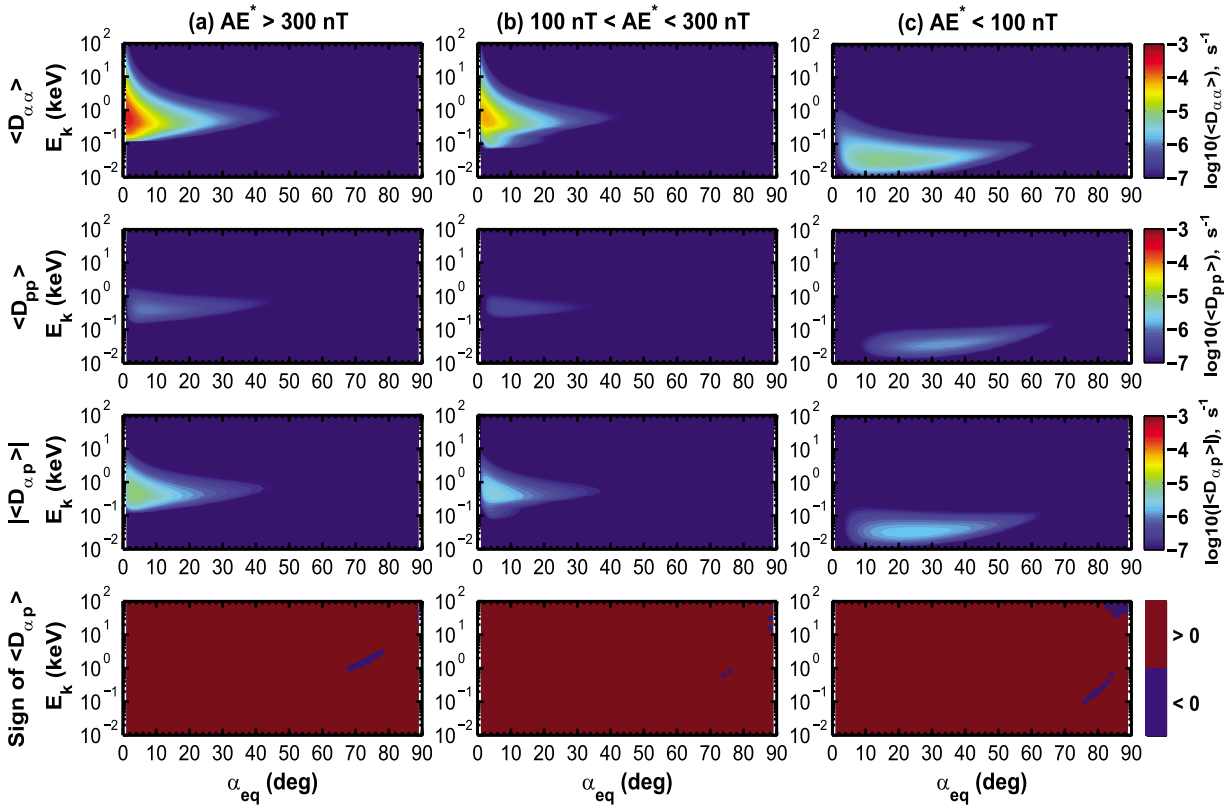

Figure 9. Net (total) bounce-averaged resonant diffusion rates ($\langle D_{\alpha\alpha}\rangle$, $|\langle D_{\alpha p}\rangle|$, $\langle D_{pp}\rangle$) as a function of both equatorial pitch angle and electron kinetic energy due to combined scattering of all four ECH harmonic bands at $L = 6$, from left to right, under active ($AE^* > 300$ nT), moderate (100 nT $< AE^* <$ 300 nT), and quiet ($AE^* < 100$ nT) conditions. The signs of $\langle D_{\alpha p}\rangle$ are shown on fourth row.

could play a significant role in the production of diffuse aurora. The study of *Meredith et al.* [2009] enables us to incorporate the statistical wave spectral properties and the wave spatial distributions into a diffusion codes to compute the rates of resonant diffusion as a function of spatial location, magnetic activity, kinetic energy, and pitch angle, and thus quantify the relative roles of these waves in the production of diffuse aurora. While *Thorne et al.* [2010] have adopted the CRRES wave data and performed an analysis of the diffuse auroral scattering by ECH waves and chorus emissions, their study was restricted to scattering at $L = 5$ under moderately disturbed conditions (100 nT < AE^* < 300 nT). In the present study, we concentrate on resonant scattering of plasma sheet electrons by ECH emissions with respect to geomagnetically quiet, moderate and active conditions, in the midnight to dawn sector (0000–0600 MLT) at a specific location of $L = 6$ representative of the peak diffuse auroral precipitation in the inner magnetosphere [*Petrinec et al.*, 1999; *Anderson et al.*, 2001; *Newell et al.*, 2009]. We present a detailed description of precisely how the modeling and the calculations are performed, including the methodology of both the wave data analysis and the modeling as well as the computational improvements in evaluating scattering rates over the earlier study of *Horne and Thorne* [2000].

[31] Our computations of ECH wave-induced bounce-averaged diffusion coefficients distinguish themselves from the earlier studies [e.g., *Lyons*, 1974; *Horne and Thorne*, 2000] in the following aspects: (1) we evaluate the scattering rates over a number of multiple harmonic frequency bands instead of at a prescribed wave frequency; (2) we adopt realistic data-based statistical information of the ECH spectral intensity and averaged electric field amplitude for each harmonic band, which varies accordingly with the level of geomagnetic activity; (3) our bounce-averaging procedure includes the ECH wave propagation effects along the field line, i.e., latitudinal variations of the wave normal angle distribution and changes of the maximum propagation latitude λ_{max} with frequency that are obtained from the HOTRAY simulations; and (4) a reasonable weighting method is introduced to average resonant electron diffusion by broadband ECH emissions. We also incorporate the averaged cold plasma density and equatorial magnetic field based on the CRRES measurements into both HOTRAY simulations and diffusion rate calculation under different geomagnetic conditions.

[32] The methodology adopted is expected to substantially improve the evaluation of bounce-averaged resonant diffusion coefficients for magnetospheric electrons in the energy range of 10 eV to 100 keV. On the other hand, we note that to obtain the latitudinal variations of wave propagation and power distribution we have adopted specific electron distributions corresponding to different geomagnetic activities for the HOTRAY simulations. Since the dispersion relation,

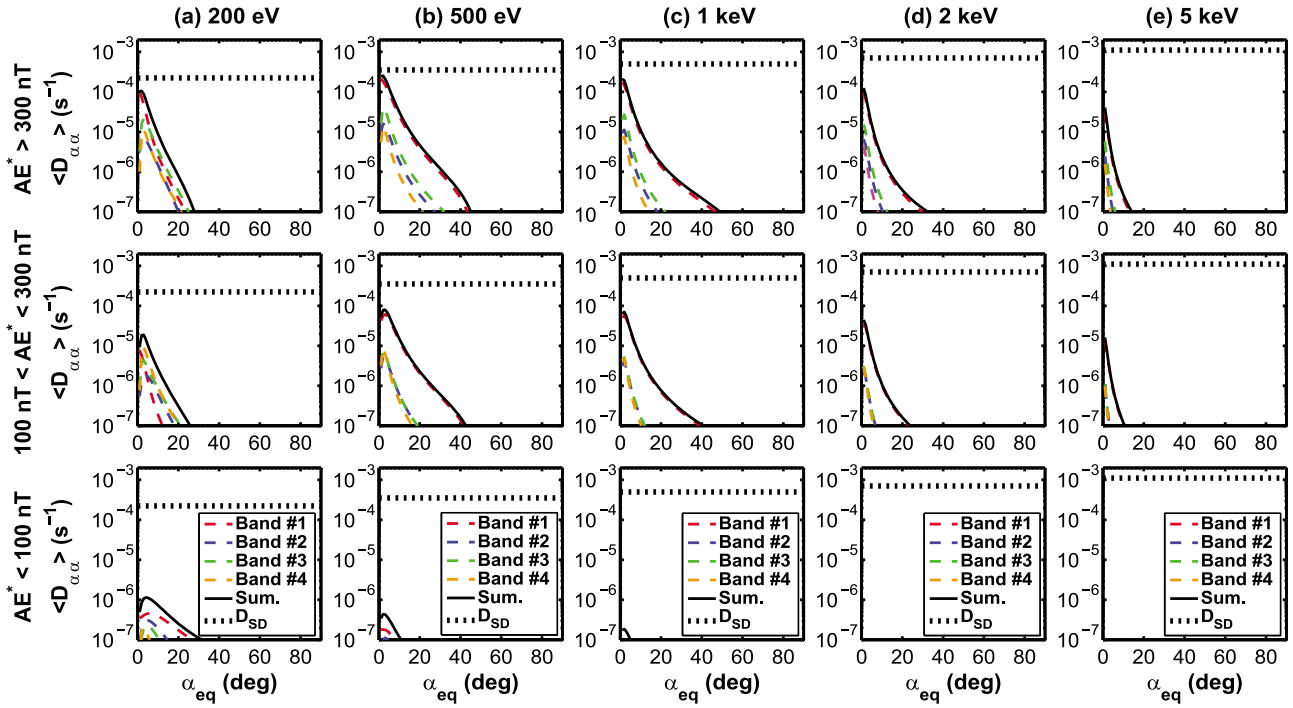

Figure 10. ECH wave-induced bounce-averaged pitch angle diffusion coefficients as a function of equatorial pitch angle, at $L = 6$, for the specified energies from 200 eV to 5 keV. Both net rates and the rates from each harmonic band are shown. The horizontal dotted line in each plot represents the strong diffusion rate D_{SD} for comparison.

excitation, and amplification of ECH waves are dependent on the distribution profiles of both cold and hot electrons, our modeled ECH wave growth and propagation can be representative but cannot be applicable to all conditions. This can explain the discrepancy between statistical results for ECH wave power distribution (Figures 1 and 2) and modeled ECH wave growth and gain variations with frequency (Figure 4). In principle, in each harmonic band lower frequency ECH waves tend to resonate with lower-energy electrons (~100 eV or lower) whose loss cone distribution can provide free energy for the excitation. Conversely, higher frequency ECH waves are more likely to be associated with higher-energy electrons (100s eV to a few keV). In our diffusion calculations, we have ignored the effects of ECH waves at the lower-edge frequency in each band (e.g., 1.1–1.2 f_{ce} for the first harmonic band) because the HOTRAY simulation yields weak growth or no excitation at these frequencies. Even though there are measurable wave intensities at these lower edge frequencies based on the CRRES statistical analysis, these waves probably correspond to conditions where the density is much lower [e.g., *Gough et al.* 1979] than the statistical average adopted in our simulations to determine the typical values of k using the HOTRAY code. We point out that accurate evaluations of both hot electron distribution function and observed frequency spectrum of wave power are important for a better understanding of the generation mechanism for ECH emissions. However, this investigation is outside the scope of the current study but will be an important topic for future investigation to establish more realistic models of ECH wave propagation during different geomagnetic conditions. We have also introduced a weighting method (equations (13) and (14)) to determine the overall diffusion coefficients due to banded ECH waves. This method is CPU efficient but results in certain inaccuracies in the diffusion rates. Combinations of the HOTRAY code (both hot plasma dispersion relation solver and ray tracer) with the general resonance finder (solving the resonance equation and ECH wave dispersion relation simultaneously) can be a promising solution to minimize the uncertainties introduced by the weighting procedure.

[33] Our calculations of resonant diffusion coefficients (Figures 9 and 10) indicate that ECH wave diffusion depends sensitively on geomagnetic activity, electron kinetic energy, and equatorial pitch angle. ECH waves generally have little effects on pitch angle scattering electrons above ~10 keV or below ~100 eV. For injected plasma sheet electrons between ~100 eV and ~10 keV that comprise the majority population for diffuse aurora, ECH emissions can cause rapid diffusion of ~200 eV to ~2 keV electrons approaching the strong diffusion limit and less efficient scattering of >2 keV electrons during geomagnetically active times. As the magnitude of geomagnetic activity decreases, the loss timescales of plasma sheet electrons by ECH waves increase correspondingly from the order of 1 h to days. Although plasma sheet electrons of 100s eV to a few keV can be scattered by ECH waves into the loss cone on a timescale of a few hours and thus contribute to the disturbed time diffuse auroral electron precipitation, the net scattering by ECH waves is confined to pitch angles $\alpha_{eq} < \sim 20°$. As a result, only a limited portion of plasma sheet electrons between 100 eV and 10 keV undergo rapid depletion through resonant interactions with ECH waves, suggesting that ECH wave scattering alone is inadequate to account for the pancake

distributions of these electrons frequently observed on the dayside, which typically exhibit a depleted electron population for $\alpha_{eq} < 70°$ that evolves from the freshly injected isotropic distributions on the timescale of the order of 4 h [*Wrenn et al.*, 1979; *Meredith et al.*, 1999, 2000; *Li et al.*, 2010]. Some other wave-particle interaction mechanism(s) is required to account for the temporal evolution of plasma sheet electrons during their nightside-to-dayside transport processes.

[34] Our present study demonstrates that multiple-harmonic ECH emissions can be partly responsible for the occurrence of diffuse auroral precipitation. A number of previous studies have suggested that whistler mode chorus might be another viable mechanism for resonant scattering plasma sheet electrons above 0.1 keV [e.g., *Inan et al.*, 1992; *Johnstone et al.*, 1993; *Villalón and Burke*, 1995; *Meredith et al.*, 1999, 2000; *Horne et al.*, 2003; *Thorne et al.*, 2010]. *Ni et al.* [2008] recently conducted a comprehensive quantitative analysis of resonant scattering of plasma sheet electrons (100 eV to 20 keV) due to resonant interactions with whistler mode chorus, proposing that upper band chorus ($0.5 < f/f_{ce} < 1.0$) is the dominant scattering process for electrons below ~5 keV while lower band chorus ($0.1 < f/f_{ce} < 0.5$) is more effective at higher energies especially near the loss cone. Furthermore, *Ni et al.* [2008] concluded that the combined scattering by upper and lower band chorus might be a major contributor to the production of diffuse aurora and the formation of electron pancake distributions. However, in the study of *Ni et al.* [2008] empirical wave characteristics, i.e., wave amplitude, frequency spectrum and wave normal angle distribution, were adopted for both lower band and upper band chorus under active conditions. To optimize the evaluations of chorus-driven bounce-averaged diffusion coefficients, as has been done here for ECH waves, we plan to utilize the CRRES wave database to construct an improved statistical wave model for both lower band and upper band chorus corresponding to different levels of geomagnetic turbulence. The statistical wave model and the determination of scattering rates of plasma sheet electrons by whistler mode chorus waves will be presented in a companion paper [*Ni et al.*, 2011], which will enable us to quantify the precise role of each wave mode in driving the diffuse auroral precipitation in the inner magnetosphere.

[35] Statistical analyses using CRRES observations capture important features of the global distribution of ECH waves, showing strong dependences on spatial location, wave frequency, and level of geomagnetic activity. However, the CRRES data coverage is limited to the inner magnetosphere, within the geocentric distances of $L = 7$. Based on an earlier survey of ECH emission using data from both the SCATHA and Active Magnetospheric Particle Tracer Explorers (AMPTE) IRM plasma wave instruments, *Roeder and Koons* [1989] showed that ECH waves can also occur in the outer magnetosphere up to 20 R_E, although intense emissions with spectral density greater than >1 μV/m/Hz$^{1/2}$ occur more frequently for $L \leq 12$. Recent observations from the THEMIS spacecraft [*Angelopoulos*, 2008] provide another useful data source to explore the global distribution of plasma waves in the outer magnetosphere. Using a 20 month data set of magnetic field filter band data from all five THEMIS spacecraft, *Li et al.* [2009] demonstrated that nightside chorus waves tend to maximize at $L < 7$ and become weaker or disappear at $L > \sim 8$. Thus, evaluations of quasi-linear resonant diffusion coefficients due to ECH waves in the outer magnetosphere are required to understand the origin of diffuse auroral precipitation at higher L shells, reported recently by *Newell et al.* [2009].

6. Principal Conclusions

[36] Using the statistical wave power spectral profiles obtained from analyzing the entire CRRES wave database and the latitudinal variations of wave normal angle distribution modeled by the HOTRAY code, we have quantitatively examined the effects of multiple-harmonic ECH emissions on resonant scattering plasma sheet electrons on the nightside for diffuse auroral precipitation under different levels of geomagnetic activity. Our principal conclusions are summarized as follows:

[37] 1. ECH wave scattering is most effective for the major population of plasma sheet electrons, between ~100 eV and a few keV, and is strongly dependent on geomagnetic activity. At $L = 6$, the resonant scattering of electrons between ~500 eV and ~2 keV by ECH waves varies from the strong diffusion limit (timescale of about an hour) during active times ($AE^* > 300$ nT) with peak wave amplitudes of the order of 1 mV/m to weak scattering (on the timescale of >1 day) during quiet conditions ($AE^* < 100$ nT) with typical wave amplitudes of tenths of mV/m.

[38] 2. Efficient ECH wave scattering, on a timescale of several hours, occurs for only a small portion of plasma sheet electrons with pitch angles $\alpha_{eq} < 30°$ for disturbed conditions and $\alpha_{eq} < 20°$ for less disturbed conditions. Consequently, multiharmonic ECH emissions cannot play a dominant role in the occurrence of diffuse auroral precipitation and the formation of electron pancake distributions [e.g., *Meredith et al.*, 1999, 2000]. Some other mechanism, such as whistler mode chorus driven resonant scattering [e.g., *Ni et al.*, 2008], is required.

[39] 3. The strongest diffusion coefficients are generally due to emissions in the first ECH harmonic band. Higher harmonic bands also contribute to resonant scattering of plasma sheet electrons, the magnitude of which largely depends on their averaged wave amplitudes relative to the first harmonic band.

[40] 4. Compared to pitch angle diffusion, ECH wave-induced momentum diffusion rates are typically 2 orders of magnitude smaller. ECH waves consequently play a negligible role in the acceleration of plasma sheet electrons.

[41] **Acknowledgments.** This research was supported by NSF grant ATM-0802843 and also by 09-LR-04116720-SHPY. The authors thank the World Data Center for Geomagnetism, Kyoto, for providing the *AE* index.

[42] Robert Lysak thanks the reviewers for their assistance in evaluating this paper.

References

Albert, J. M. (2007), Simple approximations of quasi-linear diffusion coefficients, *J. Geophys. Res.*, *112*, A12202, doi:10.1029/2007JA012551.

Anderson, P. C., S. M. Petrinec, and K. Liou (2001), Statistical patterns in X-ray and UV auroral emissions and energetic electron precipitation, *J. Geophys. Res.*, *106*(A4), 5907–5911, doi:10.1029/2000JA003041.

Anderson, R. R., D. A. Gurnett, and D. L. Odem (1992), CRRES plasma wave experiment, *J. Spacecr. Rockets*, *29*, 570–573, doi:10.2514/3.25501.

Angelopoulos, V. (2008), The THEMIS mission, *Space Sci. Rev.*, *141*, doi:10.1007/s11214-008-9336-1.

Ashour-Abdalla, M., and C. F. Kennel (1978), Nonconvective and convective electron cyclotron harmonic instabilities, *J. Geophys. Res.*, *83*(A4), 1531–1543, doi:10.1029/JA083iA04p01531.

Belmont, G., D. Fontaine, and P. Canu (1983), Are equatorial electron cyclotron waves responsible for diffuse auroral electron precipitation?, *J. Geophys. Res.*, *88*(A11), 9163–9170, doi:10.1029/JA088iA11p09163.

Chen, M. W., and M. Schulz (2001a), Simulations of storm time diffuse aurora with plasmasheet electrons in strong pitch angle diffusion, *J. Geophys. Res.*, *106*(A2), 1873–1886, doi:10.1029/2000JA000161.

Chen, M. W., and M. Schulz (2001b), Simulations of diffuse aurora with plasma sheet electrons in pitch angle diffusion less than everywhere strong, *J. Geophys. Res.*, *106*(A12), 28,949–28,966, doi:10.1029/2001JA000138.

Coroniti, F. V. (1985), Space plasma turbulent dissipation: Reality of myth?, *Space Sci. Rev.*, *42*, 399–410, doi:10.1007/BF00214995.

Fontaine, D., and M. Blanc (1983), A theoretical approach to the morphology and the dynamics of diffuse auroral zones, *J. Geophys. Res.*, *88*(A9), 7171–7184, doi:10.1029/JA088iA09p07171.

Fredricks, R. W. (1971), Plasma instability at $(n + \frac{1}{2}) f_c$ and its relationship to some satellite observations, *J. Geophys. Res.*, *76*(22), 5344–5348, doi:10.1029/JA076i022p05344.

Fredricks, R. W., and F. L. Scarf (1973), Recent studies of magnetospheric electric field emissions above the electron gyrofrequency, *J. Geophys. Res.*, *78*(1), 310–314, doi:10.1029/JA078i001p00310.

Glauert, S. A., and R. B. Horne (2005), Calculation of pitch angle and energy diffusion coefficients with the PADIE code, *J. Geophys. Res.*, *110*, A04206, doi:10.1029/2004JA010851.

Gough, M. P., P. J. Christiansen, G. Martelli, and E. J. Gershuny (1979), Interaction of electrostatic waves with warm electrons at the geomagnetic equator, *Nature*, *279*, 515–517, doi:10.1038/279515a0.

Gurnett, D. A., and A. Bhattacharjee (2005), *Introduction to Plasma Physics: With Space and Laboratory Applications*, Cambridge Univ. Press, Cambridge, U. K.

Hamlin, D. A., R. Karplus, R. C. Vik, and K. M. Watson (1961), Mirror and azimuthal drift frequencies for geomagnetically trapped particles, *J. Geophys. Res.*, *66*(1), 1–4, doi:10.1029/JZ066i001p00001.

Hardy, D. A., M. S. Gussenhoven, and E. Holeman (1985), A statistical model of auroral electron precipitation, *J. Geophys. Res.*, *90*(A5), 4229–4248, doi:10.1029/JA090iA05p04229.

Hardy, D. A., M. S. Gussenhoven, and D. Brautigam (1989), A statistical model of auroral ion precipitation, *J. Geophys. Res.*, *94*(A1), 370–392, doi:10.1029/JA094iA01p00370.

Horne, R. B. (1989), Path-integrated growth of electrostatic waves: The generation of terrestrial myriametric radiation, *J. Geophys. Res.*, *94*(A7), 8895–8909, doi:10.1029/JA094iA07p08895.

Horne, R. B., and R. M. Thorne (1993), On the preferred source location for the convective amplification of ion cyclotron waves, *J. Geophys. Res.*, *98*(A6), 9233–9247, doi:10.1029/92JA02972.

Horne, R. B., and R. M. Thorne (1994), Convective Instabilities of electromagnetic ion cyclotron waves in the outer magnetosphere, *J. Geophys. Res.*, *99*(A9), 17,259–17,273, doi:10.1029/94JA01259.

Horne, R. B., and R. M. Thorne (1997), Wave heating of He^+ by electromagnetic ion cyclotron waves in the magnetosphere: Heating near the H^+-He^+ bi-ion resonance frequency, *J. Geophys. Res.*, *102*(A6), 11,457–11,471, doi:10.1029/97JA00749.

Horne, R. B., and R. M. Thorne (2000), Electron pitch angle diffusion by electrostatic electron cyclotron harmonic waves: The origin of pancake distributions, *J. Geophys. Res.*, *105*(A3), 5391–5402, doi:10.1029/1999JA900447.

Horne, R. B., P. J. Christiansen, M. P. Gough, K. Rönnmark, J. F. E. Johnson, J. Sojka, and G. L. Wrenn (1981), Amplitude variations of electron cyclotron harmonic waves, *Nature*, *294*, 338–340, doi:10.1038/294338a0.

Horne, R. B., R. M. Thorne, N. P. Meredith, and R. R. Anderson (2003), Diffuse auroral electron scattering by electron cyclotron harmonic and whistler mode waves during an isolated substorm, *J. Geophys. Res.*, *108*(A7), 1290, doi:10.1029/2002JA009736.

Inan, U. S., Y. T. Chiu, and G. T. Davidson (1992), Whistler-mode chorus and morningside aurorae, *Geophys. Res. Lett.*, *19*(7), 653–656, doi:10.1029/92GL00402.

Johnstone, A., D. Walton, R. Liu, and D. Hardy (1993), Pitch angle diffusion of low-energy electrons by whistler mode waves, *J. Geophys. Res.*, *98*(A4), 5959–5967, doi:10.1029/92JA02376.

Kennel, C. F. (1969), Consequences of a magnetospheric plasma, *Rev. Geophys.*, *7*, 379–419, doi:10.1029/RG007i001p00379.

Kennel, C. F., and M. Ashour-Abdalla (1982), Electrostatic waves and the strong diffusion of magnetospheric electrons, in *Magnetospheric Plasma Physics*, edited by A. Nishida, pp. 245–344, Cent. for Acad. Publ., Tokyo.

Kennel, C. F., F. L. Scarf, R. W. Fredricks, J. H. McGehee, and F. V. Coroniti (1970), VLF electric field observations in the magnetosphere, *J. Geophys. Res.*, *75*(31), 6136–6152, doi:10.1029/JA075i031p06136.

Koons, H. C., and J. L. Roeder (1990), A survey of equatorial magnetospheric wave activity between 5 and 8 R_E, *Planet. Space Sci.*, *38*(10), 1335–1341, doi:10.1016/0032-0633(90)90136-E.

Li, W., R. M. Thorne, V. Angelopoulos, J. Bortnik, C. M. Cully, B. Ni, O. LeContel, A. Roux, U. Auster, and W. Magnes (2009), Global distribution of whistler-mode chorus waves observed on the THEMIS spacecraft, *Geophys. Res. Lett.*, *36*, L09104, doi:10.1029/2009GL037595.

Li, W., et al. (2010), THEMIS analysis of observed equatorial electron distributions responsible for the chorus excitation, *J. Geophys. Res.*, *115*, A00F11, doi:10.1029/2009JA014845.

Lui, A. T. Y., D. Venkatesan, C. D. Anger, S.-I. Akasofu, W. J. Heikkila, J. D. Winningham, and J. R. Burrows (1977), Simultaneous observations of particle precipitations and auroral emissions by the Isis 2 satellite in the 19–24 MLT sector, *J. Geophys. Res.*, *82*(16), 2210–2226, doi:10.1029/JA082i016p02210.

Lyons, L. R. (1974), Electron diffusion driven by magnetospheric electrostatic waves, *J. Geophys. Res.*, *79*(4), 575–580, doi:10.1029/JA079i004p00575.

Lyons, L. R., R. M. Thorne, and C. F. Kennel (1972), Pitch-angle diffusion of radiation belt electrons within the plasmasphere, *J. Geophys. Res.*, *77*(19), 3455–3474, doi:10.1029/JA077i019p03455.

Meng, C.-I., B. Mauk, and C. E. McIlwain (1979), Electron precipitation of evening diffuse aurora and its conjugate electron fluxes near the magnetospheric equator, *J. Geophys. Res.*, *84*(A6), 2545–2558, doi:10.1029/JA084iA06p02545.

Meredith, N. P., A. D. Johnstone, S. Szita, R. B. Horne, and R. R. Anderson (1999), "Pancake" electron distributions in the outer radiation belts, *J. Geophys. Res.*, *104*(A6), 12,431–12,444, doi:10.1029/1998JA900083.

Meredith, N. P., R. B. Horne, A. D. Johnstone, and R. R. Anderson (2000), The temporal evolution of electron distributions and associated wave activity following substorm injections in the inner magnetosphere, *J. Geophys. Res.*, *105*(A6), 12,907–12,917, doi:10.1029/2000JA900010.

Meredith, N. P., R. B. Horne, and R. R. Anderson (2001), Substorm dependence of chorus amplitudes: Implications for the acceleration of electrons to relativistic energies, *J. Geophys. Res.*, *106*(A7), 13,165–13,178, doi:10.1029/2000JA900156.

Meredith, N. P., R. B. Horne, R. M. Thorne, D. Summers, and R. R. Anderson (2004), Substorm dependence of plasmaspheric hiss, *J. Geophys. Res.*, *109*, A06209, doi:10.1029/2004JA010387.

Meredith, N. P., R. B. Horne, R. M. Thorne, and R. R. Anderson (2009), Survey of upper band chorus and ECH waves: Implications for the diffuse aurora, *J. Geophys. Res.*, *114*, A07218, doi:10.1029/2009JA014230.

Newell, P. T., T. Sotirelis, and S. Wing (2009), Diffuse, monoenergetic, and broadband aurora: The global precipitation budget, *J. Geophys. Res.*, *114*, A09207, doi:10.1029/2009JA014326.

Ni, B., R. M. Thorne, Y. Y. Shprits, and J. Bortnik (2008), Resonant scattering of plasma sheet electrons by whistler-mode chorus: Contribution to diffuse auroral precipitation, *Geophys. Res. Lett.*, *35*, L11106, doi:10.1029/2008GL034032.

Ni, B., R. M. Thorne, N. P. Meredith, R. B. Horne, and Y. Y. Shprits (2011), Resonant scattering of plasma sheet electrons leading to diffuse auroral precipitation: 2. Evaluation for whistler-mode chorus waves, *J. Geophys. Res.*, *116*, A04219, doi:10.1029/2010JA016233.

Paranicas, C., W. J. Hughes, H. J. Singer, and R. R. Anderson (1992), Banded electrostatic emissions observed by the CRRES plasma wave experiment, *J. Geophys. Res.*, *97*(A9), 13,889–13,898, doi:10.1029/92JA01137.

Petrinec, S. M., D. L. Chenette, J. Mobilia, M. A. Rinaldi, and W. L. Imhof (1999), Statistical X ray auroral emissions–PIXIE observations, *Geophys. Res. Lett.*, *26*(11), 1565–1568, doi:10.1029/1999GL900295.

Roeder, J. L., and H. C. Koons (1989), A survey of electron cyclotron waves in the magnetosphere and the diffuse auroral electron precipitation, *J. Geophys. Res.*, *94*(A3), 2529–2541, doi:10.1029/JA094iA03p02529.

Sandford, B. P. (1968), Variations of auroral emissions with time, magnetic activity and the solar cycle, *J. Atmos. Sol. Terr. Phys.*, *30*, 1921–1942, doi:10.1016/0021-9169(68)90001-9.

Scarf, F. L., R. W. Fredricks, C. F. Kennel, and F. V. Coroniti (1973), Satellite studies of magnetospheric substorms on August 15, 1968: 8. Ogo 5 plasma wave observations, *J. Geophys. Res.*, *78*(16), 3119–3130, doi:10.1029/JA078i016p03119.

Shaw, R. R., and D. A. Gurnett (1975), Electrostatic noise bands associated with the electron gyrofrequency and plasma frequency in the outer magnetosphere, *J. Geophys. Res.*, *80*(31), 4259–4271, doi:10.1029/JA080i031p04259.

Shprits, Y. Y., R. M. Thorne, R. B. Horne, and D. Summers (2006), Bounce-averaged diffusion coefficients for field-aligned chorus waves, *J. Geophys. Res.*, *111*, A10225, doi:10.1029/2006JA011725.

Summers, D., and R. M. Thorne (2003), Relativistic electron pitch-angle scattering by electromagnetic ion cyclotron waves during geomagnetic storms, *J. Geophys. Res.*, *108*(A4), 1143, doi:10.1029/2002JA009489.

Summers, D., B. Ni, and N. P. Meredith (2007), Timescales for radiation belt electron acceleration and loss due to resonant wave-particle interactions: 1. Theory, *J. Geophys. Res.*, *112*, A04206, doi:10.1029/2006JA011801.

Swift, D. W. (1981), Mechanisms for auroral precipitation: A review, *Rev. Geophys.*, *19*(1), 185–211, doi:10.1029/RG019i001p00185.

Thorne, R. M., B. Ni, X. Tao, R. B. Horne, and N. P. Meredith (2010), Scattering by chorus waves as the dominant cause of diffuse auroral precipitation, *Nature*, *467*, 943–946, doi:10.1038/nature09467.

Villalón, E., and W. J. Burke (1995), Pitch angle scattering of diffuse auroral electrons by whistler mode waves, *J. Geophys. Res.*, *100*(A10), 19,361–19,369, doi:10.1029/95JA01161.

Wrenn, G. L., J. F. E. Johnson, and J. J. Sojka (1979), Stable "pancake" distributions of low energy electrons in the plasma trough, *Nature*, *279*, 512–514, doi:10.1038/279512a0.

Young, T. S. T., J. D. Callen, and J. E. McCune (1973), High-frequency electrostatic waves in the magnetosphere, *J. Geophys. Res.*, *78*(7), 1082–1099, doi:10.1029/JA078i007p01082.

L. Chen, W. Li, B. Ni, Y. Y. Shprits, and R. M. Thorne, Department of Atmospheric and Oceanic Sciences, University of California, 405 Hilgard Ave., Box 951565, 7127 Math Science Bldg, Los Angeles, CA 90095-1565, USA. (bbni@atmos.ucla.edu)

R. B. Horne, and N. P. Meredith, British Antarctic Survey, High Cross, Madingley Road, Cambridge, CB3 0ET, UK.